NASA/CR—2006–214432

Dynamics Simulation Model for Space Tethers

E.M. Levin, J. Pearson, and J.C. Oldson
Star Technology and Research, Inc., Mount Pleasant, South Carolina

June 2006

The NASA STI Program Office…in Profile

Since its founding, NASA has been dedicated to the advancement of aeronautics and space science. The NASA Scientific and Technical Information (STI) Program Office plays a key part in helping NASA maintain this important role.

The NASA STI Program Office is operated by Langley Research Center, the lead center for NASA's scientific and technical information. The NASA STI Program Office provides access to the NASA STI Database, the largest collection of aeronautical and space science STI in the world. The Program Office is also NASA's institutional mechanism for disseminating the results of its research and development activities. These results are published by NASA in the NASA STI Report Series, which includes the following report types:

- TECHNICAL PUBLICATION. Reports of completed research or a major significant phase of research that present the results of NASA programs and include extensive data or theoretical analysis. Includes compilations of significant scientific and technical data and information deemed to be of continuing reference value. NASA's counterpart of peer-reviewed formal professional papers but has less stringent limitations on manuscript length and extent of graphic presentations.

- TECHNICAL MEMORANDUM. Scientific and technical findings that are preliminary or of specialized interest, e.g., quick release reports, working papers, and bibliographies that contain minimal annotation. Does not contain extensive analysis.

- CONTRACTOR REPORT. Scientific and technical findings by NASA-sponsored contractors and grantees.

- CONFERENCE PUBLICATION. Collected papers from scientific and technical conferences, symposia, seminars, or other meetings sponsored or cosponsored by NASA.

- SPECIAL PUBLICATION. Scientific, technical, or historical information from NASA programs, projects, and mission, often concerned with subjects having substantial public interest.

- TECHNICAL TRANSLATION. English-language translations of foreign scientific and technical material pertinent to NASA's mission.

Specialized services that complement the STI Program Office's diverse offerings include creating custom thesauri, building customized databases, organizing and publishing research results…even providing videos.

For more information about the NASA STI Program Office, see the following:

- Access the NASA STI Program Home Page at ***http://www.sti.nasa.gov***

- E-mail your question via the Internet to help@sti.nasa.gov

- Fax your question to the NASA Access Help Desk at 301–621–0134

- Telephone the NASA Access Help Desk at 301–621–0390

- Write to:
  NASA Access Help Desk
  NASA Center for AeroSpace Information
  7121 Standard Drive
  Hanover, MD 21076–1320
  301–621–0390

NASA/CR—2006–214432

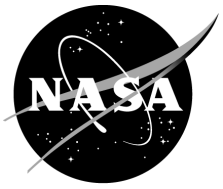

Dynamics Simulation Model for Space Tethers

E.M. Levin, J. Pearson, and J.C. Oldson
Star Technology and Research, Inc., Mount Pleasant, South Carolina

National Aeronautics and
Space Administration

Marshall Space Flight Center • MSFC, Alabama 35812

June 2006

Available from:

NASA Center for AeroSpace Information
7121 Standard Drive
Hanover, MD 21076–1320
301–621–0390

National Technical Information Service
5285 Port Royal Road
Springfield, VA 22161
703–487–4650

TABLE OF CONTENTS

TABLE OF CONTENTS (Continued)

CONTRACTOR REPORT

DYNAMICS SIMULATION MODEL FOR SPACE TETHERS

I. INTRODUCTION

The Momentum Exchange Electrodynamic Reboost (MXER) system is a rotating tether about 100 kilometers long in elliptical equatorial Earth orbit designed to catch payloads in LEO with its lower end and throw the payloads to geosynchronous transfer orbit (GTO) or to Earth escape by releasing the payloads at the top of the MXER rotation. To ensure successful rendezvous between the catcher at the MXER tip and a payload in LEO, a high-fidelity model of the system dynamics and control must be developed. This model must show that the MXER tether tip can be maneuvered precisely and at the exact time to rendezvous with and catch a payload, to within meters of positional error and within meters/second of velocity error, all at high tip acceleration.

This report deals with an investigation of the modeling of the MXER dynamics in order to provide an accurate enough representation of the MXER system and the environmental perturbations to ensure that payloads can be reliably caught and released on accurate trajectories. This allows an evaluation of the control requirements for MXER operations, the implications of operations in nonequatorial orbits, and the use of electrodynamic forces in multiple rendezvous control. We examined the accuracy of various models and the accuracy of environmental measurements required to predict the MXER tip position after one orbit, but did not deal with the requirements of electrodynamic reboosting.

II. DYNAMIC MODEL AND PERTURBATION RESPONSES

To develop effective mathematical approaches to the accurate simulation of the dynamics of a MXER tether system, we addressed two fundamental themes:

1. Identification of the MXER system dynamics and its responses to various perturbations, the relative importance of perturbing factors and environmental unknowns, and the required accuracy of the dynamic model; and
2. Based upon the understanding of the dynamic behavior of MXER, development and comparison of different computational methods to identify the most effective approach to the simulation of MXER dynamics.

The theory of pendular motions formulated in the book "Dynamics of Space Tether Systems" (1993) by Beletsky and Levin was applied to a MXER system consisting of a number of point masses connected with massive tethers of fixed lengths. Equations for determining eigenforms and eigenfrequencies of a rapidly rotating tether system were derived, leading to the equations of the excitation of eigenforms under small perturbations. Eigenforms and eigenfrequencies were computed, and the motion of a the MXER system was developed as a combination of the orbital motion of the center of mass, rotation about the center of mass, and vibrations about the line of rotation. This approach gives a very effective and clear way to describe the dynamic responses to perturbations.

A reference (unperturbed) motion near the equatorial plane was defined that results in an ideal rendezvous; the required integration accuracy was then determined for a typical rendezvous preparation period of a day or a few days.

The perturbing gravitational forces on the tether system are partly caused by the fact that the tether length is generally not small. After considering a number of analytical approaches, an expansion in a form of a polynomial series was adopted to represent the gravitational perturbations on a tether system of finite length.

The minimum number of terms in the gravitational field expansion needed to support high-precision modeling of MXER dynamics was considered. It was determined that while this number is not particularly large at the apogee, it increases dramatically at the perigee, with the amount of computation increasing proportionally to the second power of the required order of the gravitational model. A relatively simple practical formula was derived to determine the minimum required order of the gravitational field as a function of the current geocentric radius. A similar formula was derived to evaluate the minimum number of terms in the expansion of the gravitational perturbation force due to a finite (not small) spatial span of the MXER system.

Assuming linear superposition, the dynamic response to each perturbation was analyzed, including harmonics of the Earth gravitational field, interaction of the geomagnetic field with a sample current in the tether, aerodynamics, solar pressure, tether temperature variations, creep, and mass loss, to provide a richly detailed dynamic portrait of the system.

Based on the dynamic response study, we described the impact of each perturbation on the rendezvous accuracy and derive the accuracy requirements for each perturbation model. This analysis may also suggest ways to compensate for environmental unknowns with in-flight measurements.

The model based on the modal decomposition allows us to calculate the position of the MXER tether ends to the required accuracy of about 1 meter after one orbit. The results of this task, including a detailed dynamic portrait of the system, its sensitivity to perturbations, and the model accuracy requirements, provide the necessary basis for finding effective computational schemes for MXER. The complete analysis is shown in Appendix A.

III. DEVELOPMENT OF COMPUTATIONAL MODEL

The MXER dynamic model consists of multiple point masses connected in succession with fixed-length uniform tethers. We investigated convergence, stability, error accumulation, minimum number of nodes or modes, ways to compute external forces, optimal integration, maximum time step and propagation speed. Special attention was paid to the stiffness of the system caused by a drastic difference between the longitudinal and transverse wave velocities. We then compared the advantages and disadvantages of all methods and determined the most effective approach.

One of the benefits of the suggested analytical formulation is that it allows us to operate with finite formulas, and to avoid integration of the gravitational forces along the tether on each simulation step; this leads to a faster computational scheme. The minimum number of expansion terms for the required accuracy was considered.

Suitable ways of incorporating non-gravitational forces into the high-precision modal-based computational scheme were investigated. One of the goals was to avoid integration of the distributed forces along the tether on each step. It was shown that a compact set of pre-computed coefficients can be used to effectively account for distributed and concentrated forces with the required precision, assuming that the environmental models are accurate. In test runs, the computational overhead of adding the perturbation forces was not significant.

The second model used modified Minakov's equations, which are a form of second order partial differential equations with respect to the tether tension. The advantage is that they allow easier separation of fast longitudinal oscillations from the slow transverse oscillations of the tether, and therefore, they can be integrated with larger time steps.

To independently verify the results of both modal decomposition method and Minakov's method, a third model with lumped masses was developed.

The complete results of this simulation are presented in the two appendices. Assuming that the environmental parameters are known to the required precision, the modal decomposition method proved to be accurate enough to provide 9–10 digit precision in prediction of the MXER tether position over the time of one orbit, providing accuracy on the order of 1 meter in the tip position. The results show that these equations can be integrated with a time step of about 3–4 seconds of orbital time, taking only a few seconds on a standard PC to propagate a solution over one orbit with 9–10 digit precision.

IV. C++ DEMONSTRATION OF MODEL PERFORMANCE

Because of requirements for coding the equations of motion for MXER into NASA's MXER Simulation Program, we provided assistance in adapting the equations for coding at the MSFC. The requirement was for the equations to be coded, checked, and documented as an additional part of the contract. Output was provided as a text file representing a solution with predefined parameters.

We provided a computer source code from our results written as a Microsoft Visual C++ project for a Win32 console application demonstrating computational techniques involved in our high precision MXER simulation based on the modal decomposition. The source code was delivered in May of 2005, and is a separate item from this final report.

V. RESULTS

The model based on the modal decomposition of motion was used to evaluate the effects of the various perturbations on the transverse tip response. The results are shown in the table. The MXER system is extremely sensitive to temperature variations and creep, with the responses to these perturbations being 1–2 orders of magnitude higher than the others. Creep is due to the tether stress, and will be relatively constant, but the temperature response will depend on the deterioration of the tether surface, cloud cover on Earth, orbital motion and the rotation angle of MXER.

Table 1. Sensitivity to perturbations.

Perturbation	Parameter Variation	Transverse Tip
Response, Meters		
Aerodynamic	5%	2
Ampere Forces	1 mA	3
Solar Radiation Pressure	5%	1–4
Thermal Expansion	1 K	163
Creep	2.4 m/day	41
Mass Loss	5–150 g/day	< 0.001

The MXER system exhibits another surprising aspect: there is a near resonance of the main transverse mode U_2 and the frequency of the gravity gradient variation, which cycles twice every rotation of the tether system about its center of mass, or 2Ω. This is a long-term resonant effect, with the amplitude changing gradually over multiple perigee passages. The maximum tip response builds to about 120 meters over five perigee passages, then decreases to nearly zero over the next five perigee passages.

A typical response is shown in Figure 1. This resonance is difficult to avoid by changing the spin rate, because the transverse frequencies are proportional to Ω.

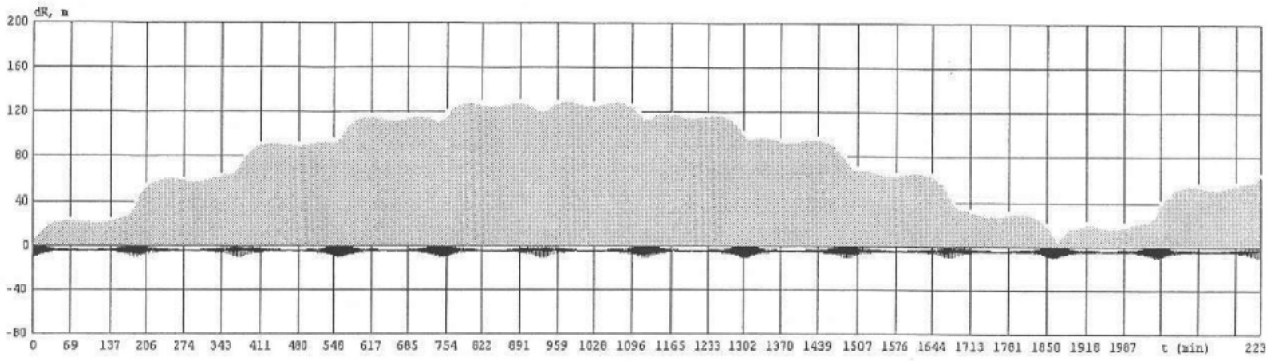

Figure 1. Transverse amplitude over twelve orbits.

VI. CONCLUSIONS AND RECOMMENDATIONS

The MXER dynamic system is very sensitive to perturbations, and is extremely sensitive to length variations. The main environmental uncertainty is temperature, which causes the largest changes in tip transverse position. It is therefore important that MXER have a very accurate estimation system, and a very accurate control system. This will require the design of estimation and control algorithms based on very accurate in-flight measurements of the distances between neighboring modules. This is a challenging task, but the distance variations carry the signatures of all the dynamic processes, and will form the basis for the control signals.

APPENDIX A—MXER SIMULATION STUDY, PART I

STAR, Inc.

MXER SIMULATION STUDY

E. M. LEVIN

Part I

Prepared for MSFC
November 17, 2005

NOMENCLATURE

A = first end-body
B = second end-body
C = center of mass of the tether system
E = longitudinal stiffness of the tether
J_C = moment of inertia of the tether system
L = total tether length
L_k = length of the k-th segment of the tether
m_A = mass of the first end-body
m_B = mass of the second end-body
m_k = embedded mass k
R = geocentric radius
R_E = mean radius of the Earth
R_C = geocentric radius of the center of mass
s = arclength along the unstretched tether
T = tether tension
t = time
γ = tether elongation
ρ = tether mass per unit length
λ = longitude
$\boldsymbol{\tau}$ = unit vector along the tether line
$\boldsymbol{\tau}_1$ = direction of the imaginary straight tether line
Ω = rotational angular rate
$(\dot{})$ = differentiation with respect to time
$(')$ = differentiation with respect to the arclength

1. FORMULATION OF THE PROBLEM

In this study, we consider the dynamics of a spinning tether system in an elliptical orbit in application to the Momentum Exchange Electrodynamic Reboost system. Momentum exchange tether systems have been studied in a variety of applications since Hans Moravec's early publication [1]. It has recently been suggested that momentum exchange systems can be enhanced with electrodynamic reboost between payload transfers [2-4].

The Momentum Exchange Electrodynamic Reboost system (MXER) has a projected tether span of up to 100 km, and spins rapidly with a period of 6-7 min. It is placed in an orbit with a low perigee of about 400 km and a high apogee of about 8000 km. To capture a payload at a perigee rendezvous, within a window of a few seconds, the motion of the system has to be predicted with very high precision, having acceptable position errors on the order of 1 m.

While this level of precision is routinely achieved today for conventional (non-tethered) satellites, it is much more difficult to achieve for a 100 km long flexible tether system. It is the goal of this study to investigate theoretical aspects of the dynamics and offer a practical approach to high precision dynamic modeling of a typical momentum exchange tether system.

2. DYNAMIC MODEL AND EQUATIONS OF MOTION

For the purposes of this study, we will assume that the momentum exchange system consists of two end-bodies A and B, modeled as point masses m_A and m_B, respectively, and a number of embedded masses m_k, $k = 1, \ldots, K$, connected with tether segments of lengths L_k, as shown in Fig. 1. Mass m_A can be counted as m_0, and mass m_B as m_{K+1}. Segment L_k connects masses m_k and m_{k+1}.

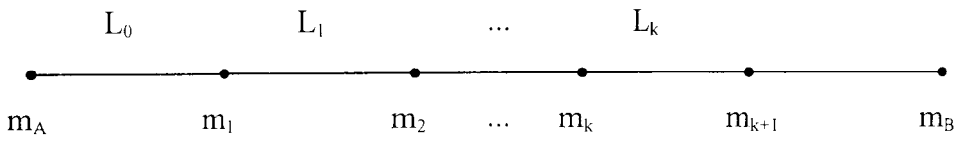

Fig. 1. Structure of the momentum exchange tether system.

All point masses and the masses of the tether segments are assumed to be constant. Tether mass per unit length can vary along the tether.

Positions of the tether elements with respect to a non-rotating geocentric reference frame $OXYZ$ are defined by the geocentric radius $\mathbf{R}$ as a function of the arclength s measured along the unstreched tether from A to B, and time t,

$$\mathbf{R} = \mathbf{R}(s,t),$$

Positions of the end masses and embedded masses are

$$\mathbf{R}_A = \mathbf{R}(s_A,t), \quad \mathbf{R}_B = \mathbf{R}(s_B,t), \quad \mathbf{R}_k = \mathbf{R}(s_k,t).$$

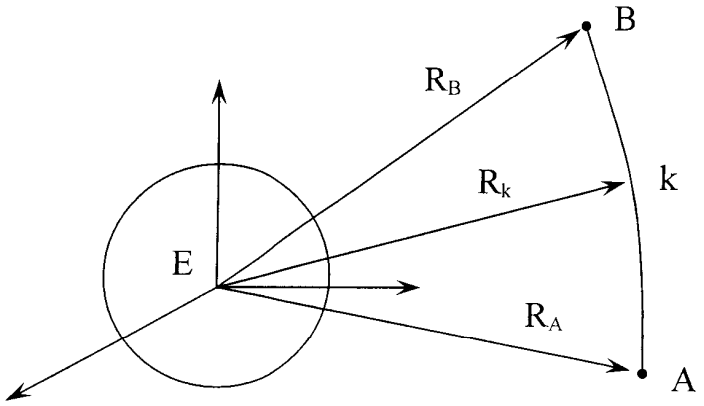

Fig. 2. Positions of the tether system elements.

The tension vector of a perfectly flexible tether is tangent to the tether line

$$\mathbf{T} = \frac{T}{\gamma}\mathbf{R}', \qquad \gamma = |\mathbf{R}'|. \tag{1}$$

where prime denotes differentiation with respect to the arclength s, and γ is the local tether elongation.

The tether tension can be expressed as a function of the elongation γ, elongation rate $\dot{\gamma}$, temperature Θ, and other factors, such as creep history,

$$T = T(s,\, t,\, \gamma,\, \dot{\gamma},\, \Theta, \ldots). \tag{2}$$

Equations of motion of the tether system constitute a mix of ordinary and partial differential equations [5]. The motion of the end masses and embedded masses is described by the ordinary differential equations

$$\begin{aligned} m_A \ddot{\mathbf{R}}_A &= \mathbf{T}_A + m_A \mathbf{g}_A + \mathbf{F}_A \\ m_B \ddot{\mathbf{R}}_B &= -\mathbf{T}_B + m_B \mathbf{g}_B + \mathbf{F}_B \\ m_k \ddot{\mathbf{R}}_k &= \mathbf{T}_{k+} - \mathbf{T}_{k-} + m_k \mathbf{g}_k + \mathbf{F}_k \end{aligned} \tag{3}$$

where dots denote differentiation with respect to time, $\mathbf{g}_A$, $\mathbf{g}_B$, and $\mathbf{g}_k$ are the gravity accelerations at points A, B, and k, respectively, $\mathbf{F}_A$, $\mathbf{F}_B$, and $\mathbf{F}_k$ are non-gravitational forces acting on the end masses and embedded masses. The tether tension vectors are taken at the following points: $\mathbf{T}_A$ at point A, $\mathbf{T}_B$ at point B, $\mathbf{T}_{k-}$ at point k of segment L_{k-1}, and $\mathbf{T}_{k+}$ at point k of segment L_k.

The motion of the tether is described by the partial differential equation

$$\rho \ddot{\mathbf{R}} = \mathbf{T}' + \rho \mathbf{g} + \mathbf{F} \tag{4}$$

where dots denote differentiation with respect to time t, and primes denote differentiation with respect to the arclength s, ρ is the tether mass per unit length, and $\mathbf{T}$ is the tether tension.

3. GRAVITATIONAL FIELD MODEL

The gravitational field is a sum of the gravitational field of the Earth and other celestial bodies, primarily, the Moon and the Sun.

The geopotential U is usually represented as

$$U = \frac{\mu_E}{R} \sum_{n=0}^{\infty} \sum_{m=0}^{n} \left(\frac{R_E}{R} \right)^n (\bar{C}_{nm} \cos m\lambda + \bar{S}_{nm} \sin m\lambda) \bar{P}_{nm}(\cos \alpha), \tag{5}$$

where μ_E is the gravitational constant of the Earth, R_E is the equatorial radius of the Earth, R is the geocentric radius, λ is the geographical longitude eastward from Greenwich, α is the geocentric colatitude (the angle between the rotation axis of the Earth and the geocentric radius of a point, $\alpha = 0$ at the North Pole), $\bar{P}_{nm}$ are normalized Legendre functions,

$$\bar{P}_{nm}(\cos \alpha) = \varkappa_n^m P_n^m(\cos \alpha),$$

$\varkappa_n^m$ is a norm,

$$\varkappa_n^0 = \sqrt{2n+1}, \qquad \text{with} \quad m = 0,$$

$$\varkappa_n^m = \sqrt{\frac{2\,(2n+1)\,(n-m)!}{(n+m)!}}, \qquad \text{with} \quad m > 0,$$

and P_n^m are associated Legendre functions of degree n and order m,

$$P_n^m(x) = (1-x^2)^{m/2}\,\frac{d^m}{dx^m}P_n(x), \qquad P_n(x) = \frac{1}{2^n n!}\frac{d^n}{dx^n}(x^2-1)^n,$$

$$P_0^0 = 1,$$

$$P_1^0(\cos\alpha) = \cos\alpha,$$

$$P_1^1(\cos\alpha) = \sin\alpha,$$

$$P_2^0(\cos\alpha) = \frac{1}{4}(3\cos 2\alpha + 1) = \frac{1}{2}(3\cos^2\alpha - 1),$$

$$P_2^1(\cos\alpha) = \frac{3}{2}\sin 2\alpha = 3\sin\alpha\cos\alpha,$$

$$P_2^2(\cos\alpha) = \frac{3}{2}(1-\cos 2\alpha) = 3\sin^2\alpha,$$

$$P_3^0(\cos\alpha) = \frac{1}{8}(5\cos 3\alpha + 3\cos\alpha) = \frac{1}{2}(5\cos^3\alpha - 3\cos\alpha),$$

$$P_3^1(\cos\alpha) = \frac{3}{8}(\sin\alpha + 5\sin 3\alpha) = \frac{3}{2}\sin\alpha(5\cos^2\alpha - 1),$$

$$P_3^2(\cos\alpha) = \frac{15}{4}(\cos\alpha - \cos 3\alpha) = 15\sin^2\alpha\cos\alpha,$$

$$P_3^3(\cos\alpha) = \frac{15}{4}(3\sin\alpha - \sin 3\alpha) = 15\sin^3\alpha,$$

...

The components of the gravitational acceleration $\mathbf{g} = \nabla U$ are

$$g_R = \frac{\partial U}{\partial R}, \qquad g_\alpha = \frac{1}{R}\frac{\partial U}{\partial \alpha}, \qquad g_\lambda = \frac{1}{R\sin\alpha}\frac{\partial U}{\partial \lambda},$$

where g_R is pointing along the geocentric radius, g_α is pointing southward along the meridian, and g_λ is pointing eastward along the parallel. In the geocentric axes OXYZ,

$$g_x = (g_R\cos\varphi + g_\alpha\sin\varphi)\cos\lambda - g_\lambda\sin\lambda$$

$$g_y = (g_R\cos\varphi + g_\alpha\sin\varphi)\sin\lambda + g_\lambda\cos\lambda$$

$$g_z = g_R\sin\varphi - g_\alpha\cos\varphi$$

where $\varphi = \pi/2 - \alpha$ is the latitude.

To properly evaluate convergence, we should use a geopotential model of the maximum available degree and order. An obvious choice is the Earth Gravity Model EGM96 [6], of degree and order 360.

According to this model, $\mu_E = 398600.4415$ km^3/sec^2, $R_E = 6378.1363$ km, and the normalized coefficients $\bar{C}_{nm}$ and $\bar{S}_{nm}$ are as follows:

$$\bar{C}_{0,0} = 1, \qquad \bar{S}_{0,0} - \text{not used}$$
$$\bar{C}_{1,0} = 0, \qquad \bar{S}_{1,0} - \text{not used}$$
$$\bar{C}_{1,1} = 0, \qquad \bar{S}_{1,1} = 0,$$
$$\bar{C}_{2,0} = -0.484165371736 \cdot 10^{-3}, \qquad \bar{S}_{2,0} - \text{not used}$$
$$\bar{C}_{2,1} = -0.186987635955 \cdot 10^{-9}, \qquad \bar{S}_{2,1} = 0.119528012031 \cdot 10^{-8},$$
$$\bar{C}_{2,2} = 0.243914352398 \cdot 10^{-5}, \qquad \bar{S}_{2,2} = -0.140016683654 \cdot 10^{-5},$$
$$\bar{C}_{3,0} = 0.957254173792 \cdot 10^{-6}, \qquad \bar{S}_{3,0} - \text{not used}$$
$$\bar{C}_{3,1} = 0.202998882184 \cdot 10^{-5}, \qquad \bar{S}_{3,1} = 0.248513158716 \cdot 10^{-6},$$
$$\bar{C}_{3,2} = 0.904627768605 \cdot 10^{-6}, \qquad \bar{S}_{3,2} = -0.619025944205 \cdot 10^{-6},$$
$$\bar{C}_{3,3} = 0.721072657057 \cdot 10^{-6}, \qquad \bar{S}_{3,3} = 0.141435626958 \cdot 10^{-5},$$
$$\ldots \qquad \ldots$$
$$\bar{C}_{360,359} = 0.183971631467 \cdot 10^{-10}, \qquad \bar{S}_{360,359} = -0.310123632209 \cdot 10^{-10},$$
$$\bar{C}_{360,360} = -0.447516389678 \cdot 10^{-24}, \qquad \bar{S}_{360,360} = -0.830224945525 \cdot 10^{-10}$$

Gravitational perturbations caused by the Earth tides can be described by time dependent variations in the geopotential expansion coefficients [7].

Gravitational perturbations caused by a celestial body of mass M_p located at $\mathbf{R}_p$ with respect to the geocentric axes $OXYZ$ are described as

$$\mathbf{g}_p = GM_p \left(\frac{\mathbf{R}_p - \mathbf{R}}{|\mathbf{R}_p - \mathbf{R}|^3} - \frac{\mathbf{R}_p}{R_p^3} \right), \tag{6}$$

where G is the universal gravity constant, and $R_p = |\mathbf{R}_p|$.

For most practical purposes and for all celestial bodies, except the Moon, the linear approximation

$$\mathbf{g}_p = \frac{GM_p}{R_p^3} [3\mathbf{e}_p(\mathbf{e}_p, \mathbf{R}) - \mathbf{R}], \tag{7}$$

where $\mathbf{e}_p = \mathbf{R}_p / R_p$ is a unit vector of the direction to the celestial body, should be adequate [7].

4. STATIONARY ROTATION

If we disregard non-gravitational forces $\mathbf{F}$ in equations (3)–(4) and assume that the tether is inextensible ($\gamma = |\mathbf{R}'| = 1$) and gravitational acceleration does not vary along the tether ($\mathbf{g} = \mathbf{g}_C$), then equations (3)–(4) will have a stationary solution

$$\mathbf{T} = T(s)\,\boldsymbol{\tau}(t), \qquad \mathbf{R} = \mathbf{R}_C(t) + (s - s_C)\,\boldsymbol{\tau}(t), \tag{8}$$

where $\mathbf{R}_C(t)$ and $\boldsymbol{\tau}(t)$ are determined from

$$\ddot{\mathbf{R}}_C = \mathbf{g}_C, \qquad \ddot{\boldsymbol{\tau}} = -\Omega^2\,\boldsymbol{\tau}. \tag{9}$$

Here, $\mathbf{R}_C$ is the radius-vector of the center of mass, moving as a point mass, $\mathbf{g}_C$ is the gravity acceleration at the center of mass, $\boldsymbol{\tau}$ is a unit vector along the tether line rotating at a constant angular velocity $\boldsymbol{\Omega}$ in a fixed plane normal to $\boldsymbol{\Omega}$, $\Omega = |\boldsymbol{\Omega}|$, s_C is the arclength corresponding to the center of mass

$$s_C = \frac{1}{M}\left(m_A s_A + m_B s_B + \sum_k m_k s_k + \int_A^B \rho\, s\, ds\right), \tag{10}$$

and M is the total mass of the tether system.

In the stationary motion (8)–(9), we have

$$\ddot{\mathbf{R}} = \ddot{\mathbf{R}}_C + (s - s_C)\,\ddot{\boldsymbol{\tau}} = \mathbf{g}_C - (s - s_C)\,\Omega^2\boldsymbol{\tau}.$$

After substituting this relation into equations (3)–(4), we arrive at a boundary problem for the equilibrium tension,

$$\begin{aligned} T' &= -\rho\,\Omega^2(s - s_C), \\ T_A &= -m_A\Omega^2(s_A - s_C), \\ T_B &= m_B\Omega^2(s_B - s_C), \\ T_{k+} &= T_{k-} - m_k\Omega^2(s_k - s_C), \end{aligned} \tag{11}$$

where the last equation defines tension increments associated with the embedded masses m_k.

The equilibrium tension is obtained by solving the first equation of (11) with the initial condition $T = T_A$ given by the second equation and incrementing the tension at the points s_k, as described by the last equation of (11). The boundary

condition $T = T_B$ given by third equation is always satisfied because of the definition of the value s_C (10) and the structure of equations (11).

In general, the equilibrium tension increases from the value T_A at the end A to its maximum value T_C at the center of mass C, and then drops to the value T_B at the other end, as shown in Fig. 3.

To minimize mass, the tether should be tapered, with the linear density varying along the tether, $\rho = \rho(s)$. Ideally, the tether should be equally stressed/strained at all points,

$$\frac{T}{E} = \delta_*, \tag{12}$$

where E is the longitudinal tether stiffness, and δ_* is the maximum allowed strain. Condition (12) can be rewritten as

$$T = \rho\, v_E^2\, \delta_*, \qquad v_E = \sqrt{\frac{E}{\rho}}, \tag{13}$$

where v_E is the longitudinal wave velocity in the tether. Now, we can express the linear density as a function of tension, $\rho = T\, v_E^{-2}\, \delta_*^{-1}$, and substitute this relation into the first equation of the boundary problem (11) to produce a boundary problem for an ideal equally stressed/strained tether.

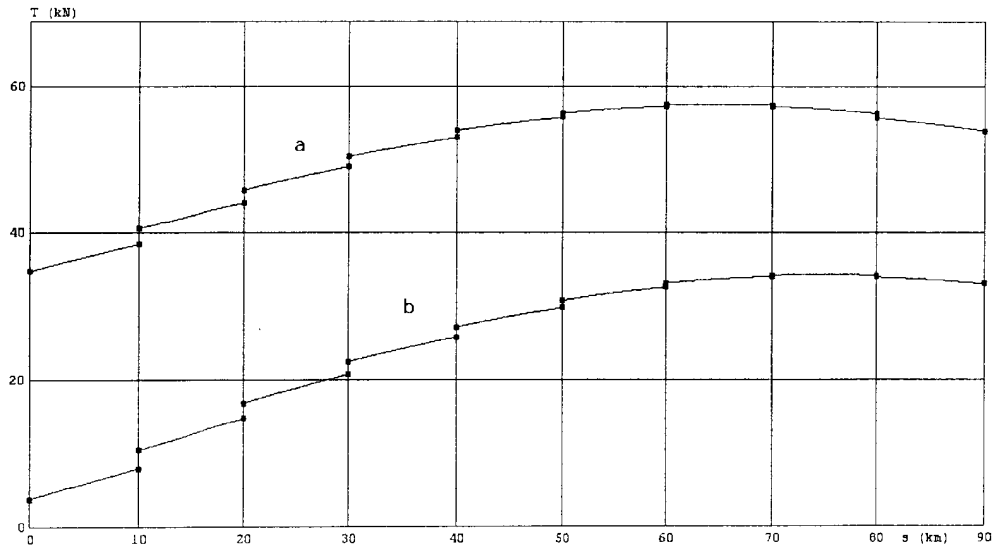

Fig. 3. Tension profile of a tether system with (a) and without (b) payload.

In practice, the tether can be made of a number of uniform segments, approximating the desired taper profile.

Typical tension profiles are shown in Fig. 3 for a 90 km tether system with $m_A = 250$ kg, $m_B = 11000$ kg, and 8 embedded masses $m_k = 200$ kg placed 10 km apart. The tethers are made of Zylon and are uniform on each segment with a maximum strain of $\delta_* = 0.01$. The system spins at $\Omega = 0.8$ deg/sec. In case (a), the end mass A carries a 2500 kg payload, and there is no payload in case (b).

5. SMALL OSCILLATIONS AND EIGENFORMS

To study small oscillations of the tether system about the stationary rotation, we introduce a rotating reference frame $C\xi\eta\zeta$, with the origin at the center of mass, axis $C\xi$ aligned with the tether line, and axis $C\zeta$ aligned with the angular rate vector $\mathbf{\Omega}$, so that

$$\tau = (1,\, 0,\, 0), \qquad \mathbf{\Omega} = (0,\, 0,\, \Omega).$$

With respect to the rotating axes $C\xi\eta\zeta$, the stationary motion (8)–(9) is viewed as a relative equilibrium.

Equations of small oscillations of the tether system about the relative equilibrium are derived from (3)–(4),

$$\begin{aligned} &\rho\, D(\delta\mathbf{r}) = \delta\mathbf{T}', \\ &m_A\, D(\delta\mathbf{r}_A) = \delta\mathbf{T}_A, \\ &m_B\, D(\delta\mathbf{r}_B) = -\delta\mathbf{T}_B, \\ &m_k\, D(\delta\mathbf{r}_k) = \delta\mathbf{T}_{k+} - \delta\mathbf{T}_{k-}, \end{aligned} \tag{14}$$

where $\delta\mathbf{r}$ and $\delta\mathbf{T}$ are deviations from the relative equilibrium, and D denotes the linear expression

$$D(\delta\mathbf{r}) = \delta\ddot{\mathbf{r}} + 2\mathbf{\Omega} \times \delta\dot{\mathbf{r}} + \mathbf{\Omega} \times (\mathbf{\Omega} \times \delta\mathbf{r}),$$

in which derivatives are calculated with respect to the rotating axes $C\xi\eta\zeta$.

Small oscillations (14) have two independent components. One is normal to the tether line in the plane of the stationary rotation,

$$\delta\mathbf{r} = (0,\, \eta,\, 0), \qquad \delta\mathbf{T} = (0,\, T\eta',\, 0),$$

and the other one is normal to the rotation plane

$$\delta\mathbf{r} = (0,\, 0,\, \zeta), \qquad \delta\mathbf{T} = (0,\, 0,\, T\zeta').$$

There is no longitudinal component in the linear approximation for an inextensible tether.

Equations of small in-plane oscillations take the form

$$\begin{aligned}
&\rho\,(\ddot{\eta} - \Omega^2\eta) = (T\eta')',\\
&m_A\,(\ddot{\eta}_A - \Omega^2\eta_A) = (T\eta')_A,\\
&m_B\,(\ddot{\eta}_B - \Omega^2\eta_B) = -(T\eta')_B,\\
&m_k\,(\ddot{\eta}_k - \Omega^2\eta_k) = (T\eta')_{k+} - (T\eta')_{k-},
\end{aligned} \tag{15}$$

After substituting $\eta = U_n(s)\,cos(\Omega_n t)$ into (15), we arrive at the following eigenvalue problem,

$$\begin{aligned}
&(TU_n')' = -\rho\,(\Omega_n^2 + \Omega^2)\,U_n,\\
&(TU_n')_A = -m_A\,(\Omega_n^2 + \Omega^2)\,U_{nA},\\
&(TU_n')_B = m_B\,(\Omega_n^2 + \Omega^2)\,U_{nB},\\
&(TU_n')_{k+} = (TU_n')_{k-} - m_k\,(\Omega_n^2 + \Omega^2)\,U_{nk},
\end{aligned} \tag{16}$$

Small out-of-plane oscillations are described by

$$\begin{aligned}
&\rho\,\ddot{\zeta} = (T\zeta')',\\
&m_A\,\ddot{\zeta}_A = (T\zeta')_A,\\
&m_B\,\ddot{\zeta}_B = -(T\zeta')_B,\\
&m_k\,\ddot{\zeta}_k = (T\zeta')_{k+} - (T\zeta')_{k-}.
\end{aligned} \tag{17}$$

After substituting $\zeta = U_n(s)\,cos(\Omega_n t)$ into (17), we derive the following eigenvalue problem,

$$\begin{aligned}
&(TU_n')' = -\rho\,\Omega_n^2\,U_n,\\
&(TU_n')_A = -m_A\,\Omega_n^2\,U_{nA},\\
&(TU_n')_B = m_B\,\Omega_n^2\,U_{nB},\\
&(TU_n')_{k+} = (TU_n')_{k-} - m_k\,\Omega_n^2\,U_{nk}.
\end{aligned} \tag{18}$$

The eigenvalue problems (16) and (18) are very similar. They have the same eigenfunctions $U_n(s)$, and their eigenfrequencies are bound by a simple relation,

$$\Omega_{n\zeta}^2 = \Omega_{n\eta}^2 + \Omega^2. \tag{19}$$

Analyzing the boundary problem (11) for the equilibrium tension and the eigenvalue problems (16), (18), we note that the eigenforms do not depend on the angular rate Ω. Indeed, we can introduce a normalized equilibrium tension

$$P(s) = \frac{T(s)}{\Omega^2}, \tag{20}$$

and rewrite equations (11) as

$$\begin{aligned} P' &= -\rho\,(s - s_C), \\ P_A &= -m_A(s_A - s_C), \\ P_B &= m_B(s_B - s_C), \\ P_{k+} &= P_{k-} - m_k(s_k - s_C), \end{aligned} \tag{21}$$

while equations (16) and (18) can be reduced to

$$\begin{aligned} (PU_n')' &= -\rho\,\beta_n^2\,U_n, \\ (PU_n')_A &= -m_A\,\beta_n^2\,U_{nA}, \\ (PU_n')_B &= m_B\,\beta_n^2\,U_{nB}, \\ (PU_n')_{k+} &= (PU_n')_{k-} - m_k\,\beta_n^2\,U_{nk}, \end{aligned} \tag{22}$$

where β_n are dimensionless eigenvalues. The resulting system of equations (21)–(22) and its solutions do not depend on the angular rate Ω.

The eigenfrequencies $\Omega_{n\eta}$ and $\Omega_{n\zeta}$ can be expressed through the dimensionless eigenvalues β_n as

$$\Omega_{n\eta} = \sqrt{\beta_n^2 - 1}\;\Omega, \qquad \Omega_{n\zeta} = \beta_n \Omega. \tag{23}$$

The eigenvalue problem (21)–(22) has two trivial solutions,

$$\beta_0 = 0, \qquad U_0 = 1, \tag{24}$$

and

$$\beta_1 = 1, \qquad U_1 = s - s_C. \tag{25}$$

The first solution simply reduces the right and the left parts of (22) to zero, while the second solution reduces (22) to (21). Dynamically, solution (24) corresponds to perturbations of the motion of the center of mass, while solution (25) corresponds to variations of the angular rate and direction of the axis of the stationary rotation.

The trivial solutions are followed by an infinite series of solutions $\{\beta_n, U_n\}$, $n = 2, 3, \ldots$, which constitute an orthogonal basis with the orthogonality condition

$$\langle U_i, U_j \rangle = 0, \qquad i \neq j, \tag{26}$$

where

$$\langle U_i, U_j \rangle = m_A(U_iU_j)_A + m_B(U_iU_j)_B + \sum_k m_k(U_iU_j)_k + \int_A^B \rho\,(U_iU_j)\,ds. \tag{27}$$

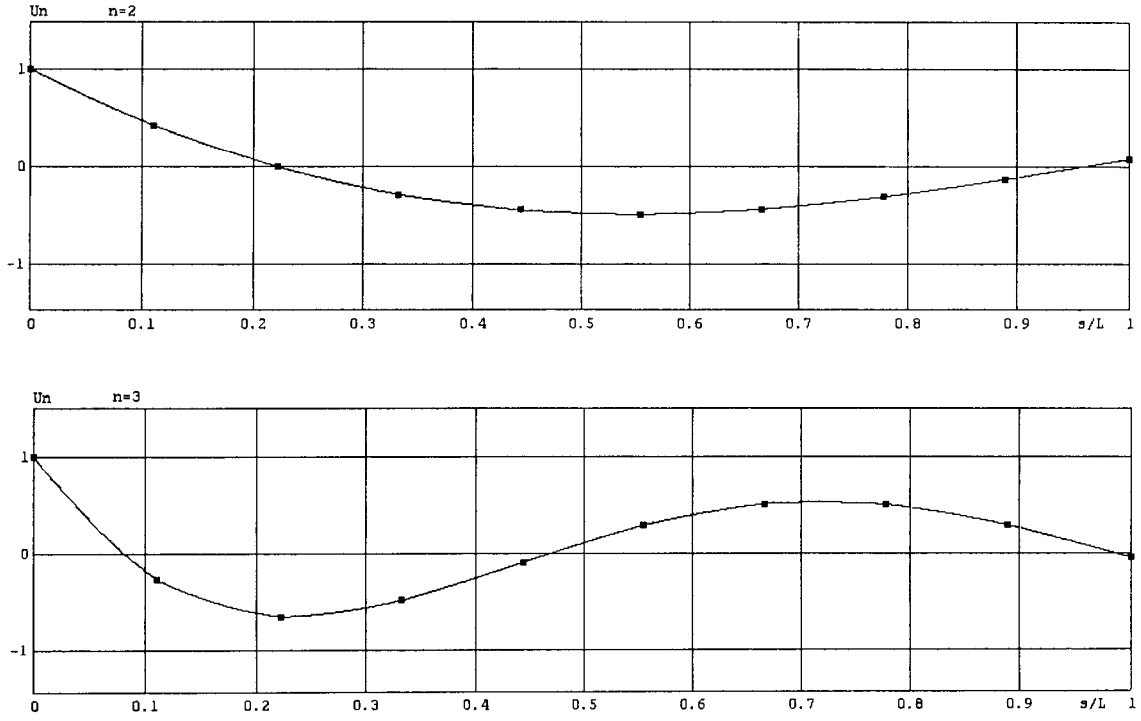

Fig. 4. Lower eigenforms of a spinning tether system ($n = 2, 3$).

The orthogonality condition can also be expressed as

$$\int_A^B P\, U_i' U_j'\, ds = 0, \qquad i \neq j. \tag{28}$$

The norms of the eigenfunctions are defined as

$$||U_n|| = \langle U_n, U_n \rangle. \tag{29}$$

The norm of the first trivial eigenfunction (24) is equal to the total mass of the tether system

$$||U_0|| = M = m_A + m_B + \sum_k m_k + \int_A^B \rho\, ds, \tag{30}$$

while the norm of the second trivial eigenfunction (25) is equal to the moment of inertia about the center of mass,

$$||U_1|| = J_C =$$

$$m_A (s_A - s_C)^2 + m_B (s_B - s_C)^2 + \sum_k m_k (s_k - s_C)^2 + \int_A^B \rho (s - s_C)^2 ds. \tag{31}$$

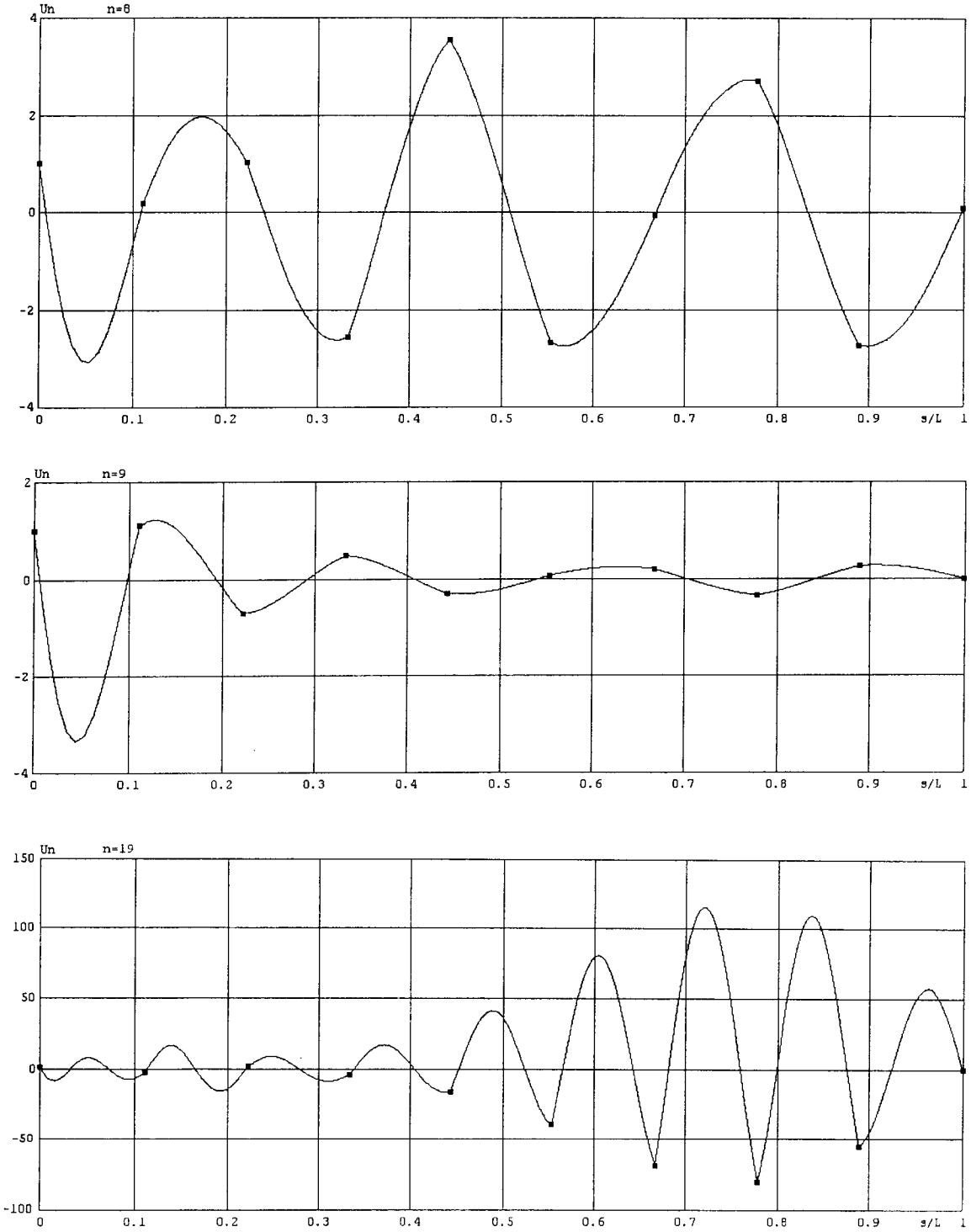

Fig. 5. Higher eigenforms of a spinning tether system ($n = 8, 9, 19$).

Also, the following relation for the eigenvalues can be derived from (22)

$$\beta_n^2 = \frac{1}{||U_n||} \int_A^B P\,(U_n')^2\,ds = 0. \tag{32}$$

Some eigenforms are shown in Fig. 4-5 for the same parameters as in case (b) of Fig. 3, namely, $L = 90$ km, $m_A = 250$ kg, $m_B = 11000$ kg, $m_k = 200$ kg, $k = 1,\ldots,8$, connected with 10 km long uniform tethers of the following masses: 318, 365, 406, 438, 461, 473, 475, 473, 460 kg. The corresponding nontrivial eigenvalues ($n = 2,\ldots,19$) are given below

$\beta_2 = 2.136,$	$\beta_8 = 10.497,$	$\beta_{14} = 20.182,$
$\beta_3 = 3.339,$	$\beta_9 = 11.355,$	$\beta_{15} = 20.573,$
$\beta_4 = 4.590,$	$\beta_{10} = 12.414,$	$\beta_{16} = 22.015,$
$\beta_5 = 5.912,$	$\beta_{11} = 15.549,$	$\beta_{17} = 23.714,$
$\beta_6 = 7.328,$	$\beta_{12} = 18.020,$	$\beta_{18} = 25.550,$
$\beta_7 = 8.853,$	$\beta_{13} = 19.320,$	$\beta_{19} = 27.529.$

Generally, the n-th form has n nodes. Note that while the lower modes (Fig. 4) show smooth curves of average collective behavior, the higher modes (Fig. 5) exhibit a more peculiar interplay between the tether and embedded mass dynamics.

6. DECOMPOSITION OF MOTION

Using eigenforms obtained from the solution of the boundary problem (21) and the eigenvalue problem (22) for a simplified case of a stationary rotation, we can represent solutions of the general equations (3)–(4) in the form of a series expansion

$$\mathbf{R}(s,t) = \sum_{n=0}^{\infty} \mathbf{q}_n(t)\,U_n(s), \tag{33}$$

where the term $n = 0$ (trivial form $U_0 = 1$) represents, in essence, the orbital motion of the center of mass, $\mathbf{q}_0 = \mathbf{R}_C(t)$, and the term $n = 1$ (trivial form $U_1 = s - s_C$) describes a quasi-rigid rotation of an imaginary straight tether, $\mathbf{q}_1 = \boldsymbol{\tau}_1(t)$, where $\boldsymbol{\tau}_1$ is pointing along the imaginary straight tether line, so that

$$\mathbf{R}(s,t) = \mathbf{R}_C(t) + (s - s_C)\,\boldsymbol{\tau}_1(t) + \sum_{n=2}^{\infty} \mathbf{q}_n(t)\,U_n(s). \tag{34}$$

The higher order terms $n \geq 2$ represent tether oscillations about the imaginary straight line drawn through the center of mass C along vector $\boldsymbol{\tau}_1$. Kinematically, they do not contribute to the displacement of the center of mass and the quasi-rigid rotation because of the orthogonality conditions (26).

Note that the term with $\boldsymbol{\tau}_1$ also describes a uniform elongation of the tether system. If we disregard the higher order terms $n \geq 2$, then the tether elongation $\gamma = |\mathbf{R}'| = |\boldsymbol{\tau}_1| = \gamma_1$ will be the same for all tether elements.

Expression (33) yields similar kinematic and dynamic relations,

$$\dot{\mathbf{R}}(s,t) = \sum_{n=0}^{\infty} \dot{\mathbf{q}}_n(t)\, U_n(s), \qquad \ddot{\mathbf{R}}(s,t) = \sum_{n=0}^{\infty} \ddot{\mathbf{q}}_n(t)\, U_n(s), \tag{35}$$

or in terms of (34),

$$\begin{aligned} \dot{\mathbf{R}}(s,t) &= \dot{\mathbf{R}}_C(t) + (s - s_C)\,\dot{\boldsymbol{\tau}}_1(t) + \sum_{n=2}^{\infty} \dot{\mathbf{q}}_n(t)\, U_n(s), \\ \ddot{\mathbf{R}}(s,t) &= \ddot{\mathbf{R}}_C(t) + (s - s_C)\,\ddot{\boldsymbol{\tau}}_1(t) + \sum_{n=2}^{\infty} \ddot{\mathbf{q}}_n(t)\, U_n(s), \end{aligned} \tag{36}$$

where the derivatives are calculated with respect to the non-rotating geocentric frame $OXYZ$.

We can now substitute the second equation of (35) into the general equations (3)–(4), multiply by U_n, $n = 0, 1, 2, \ldots$, and sum over all tether elements and point masses. Applying the orthogonality conditions (26), we find that

$$\ddot{\mathbf{q}}_n = \frac{1}{||U_n||}\,(\mathbf{Q}_n + \mathbf{G}_n + \boldsymbol{\Phi}_n), \qquad n = 0, 1, 2, \ldots, \tag{37}$$

where $\mathbf{Q}_n$ is reduced to an integral of tension,

$$\begin{aligned} \mathbf{Q}_n &= \mathbf{T}_A U_{nA} - \mathbf{T}_B U_{nB} + \sum_k (\mathbf{T}_{k+} - \mathbf{T}_{k-})\, U_{nk} + \int_A^B \mathbf{T}' U_n\, ds \\ &= -\int_A^B \mathbf{T}\, U_n'\, ds, \end{aligned} \tag{38}$$

$\mathbf{G}_n$ is expressed through the inner product (27),

$$\begin{aligned} \mathbf{G}_n &= \langle \mathbf{g},\, U_n \rangle \\ &= m_A(\mathbf{g}\, U_n)_A + m_B(\mathbf{g}\, U_n)_B + \sum_k m_k(\mathbf{g}\, U_n)_k + \int_A^B \rho\,(\mathbf{g}\, U_n)\, ds, \end{aligned} \tag{39}$$

and $\mathbf{\Phi}_n$ is a generalized sum of non-gravitational forces,

$$\mathbf{\Phi}_n = \mathbf{F}_A U_{nA} + \mathbf{F}_B U_{nB} + \sum_k \mathbf{F}_k U_{nk} + \int_A^B \mathbf{F}\, U_n\, ds. \tag{40}$$

The system of ordinary differential equations (37) is equivalent to the original system of mixed partial and ordinary differential equations (3)–(4), because it is derived through the general transformation of variables (33) without any simplifying assumptions.

Using notations (34), and taking into account that $||U_0|| = M$ and $\mathbf{Q}_0$ vanishes because $U_0' = 0$, the motion of the center of mass is described by

$$\ddot{\mathbf{R}}_C = \frac{1}{M}\,(\mathbf{G}_0 + \mathbf{\Phi}_0). \tag{41}$$

Taking into account that $||U_1|| = J_C$ and $U_1' = 1$, the quasi-rigid rotation and uniform elongation are described by

$$\ddot{\boldsymbol{\tau}}_1 = \frac{1}{J_C}\,(\mathbf{Q}_1 + \mathbf{G}_1 + \mathbf{\Phi}_1), \qquad \mathbf{Q}_1 = -\int_A^B \mathbf{T}\, ds. \tag{42}$$

According to (34), the tangent to the tether line is defined as

$$\mathbf{R}' = \boldsymbol{\tau}_1 + \Delta\boldsymbol{\tau}, \qquad \Delta\boldsymbol{\tau} = \sum_{n=2}^{\infty} \mathbf{q}_n U_n'. \tag{43}$$

Assuming that $|\Delta\boldsymbol{\tau}| \ll |\boldsymbol{\tau}_1|$, the elongation can be approximated as

$$\gamma = |\mathbf{R}'| = \sqrt{|\boldsymbol{\tau}_1|^2 + 2(\boldsymbol{\tau}_1, \Delta\boldsymbol{\tau}) + |\Delta\boldsymbol{\tau}|^2} \approx \gamma_1 + (\mathbf{e}_1, \Delta\boldsymbol{\tau}) = \gamma_1 + \sum_{n=2}^{\infty} q_{en}\, U_n', \tag{44}$$

where

$$\gamma_1 = |\boldsymbol{\tau}_1|, \qquad \mathbf{e}_1 = \frac{\boldsymbol{\tau}_1}{\gamma_1}, \qquad q_{en} = (\mathbf{e}_1, \mathbf{q}_n). \tag{45}$$

The tether tension depends not only on the elongation, but also on temperature, internal friction, creep history, and other factors. The following expression can be adopted within a certain range of conditions,

$$T = T_0 + E\,(\gamma - \gamma_*) + D\,\dot{\gamma}, \tag{46}$$

where T_0 is a reference tension, E is the tether longitudinal stiffness, D is the damping coefficient,

$$\gamma_* = \gamma_0 + \varepsilon\,(t - t_0) + \alpha\,(\Theta - \Theta_0), \tag{47}$$

γ_0 is the elongation under the reference tension T_0 at time t_0 and a reference temperature Θ_0, ε is the creep rate, α is the thermal expansion coefficient, and Θ is the current temperature of the tether element. Other terms can be added as needed.

Substituting (44) into (46), we derive

$$T = T_1 + \sum_{n=2}^{\infty} (E\, q_{en} + D\, \dot{q}_{en})\, U_n', \qquad T_1 = T_0 + E\,(\gamma_1 - \gamma_*) + D\,\dot{\gamma}_1, \tag{48}$$

and then calculate

$$\frac{T}{\gamma} \approx \frac{T_1}{\gamma_1} + \frac{1}{\gamma_1} \sum_{n=2}^{\infty} \left[\left(E - \frac{T_1}{\gamma_1} \right) q_{en} + D\, \dot{q}_{en} \right] U_n'. \tag{49}$$

Retaining only linear terms in $\mathbf{q}_n$, the integral of tension $\mathbf{Q}_n$ can now be represented as

$$\begin{aligned} \mathbf{Q}_n &= -\int_A^B \frac{T}{\gamma}\, \mathbf{R}'\, U_n'\, ds = -\int_A^B \frac{T}{\gamma} \left(\boldsymbol{\tau}_1 + \sum_{k=2}^{\infty} \mathbf{q}_k\, U_k' \right) U_n'\, ds \\ &\approx -\int_A^B \left(T_1 \mathbf{e}_1 + \sum_{k=2}^{\infty} \mathbf{c}_k\, U_k' \right) U_n'\, ds, \end{aligned} \tag{50}$$

where $\mathbf{e}_1 = \boldsymbol{\tau}_1/\gamma_1$ is a unit vector along the imaginary straight tether line and

$$\mathbf{c}_n = E\, \mathbf{e}_1 q_{en} + D\, \mathbf{e}_1 \dot{q}_{en} + \frac{T_1}{\gamma_1} (\mathbf{q}_n - \mathbf{e}_1 q_{en}), \qquad q_{en} = (\mathbf{e}_1,\, \mathbf{q}_n). \tag{51}$$

Expression (50) can be significantly simplified in the ideal case of a perfectly tapered tether. Let us define the tether reference state $T_0(s)$ as a stationary rotation at an angular rate Ω_0 free of external torques, as described in Section 4, with the exception that the tether is now elastic. Let us assume that the tether is perfectly tapered so that all tether elements have the same elongation γ_0 under the stationary tension T_0 at a given temperature Θ_0. Then, similarly to (11), the equilibrium tension profile can be determined from the boundary problem

$$\begin{aligned} T' &= -\rho\, \Omega^2 (s - s_C)\, \gamma_0, \\ T_A &= -m_A \Omega^2 (s_A - s_C)\, \gamma_0, \\ T_B &= m_B \Omega^2 (s_B - s_C)\, \gamma_0, \\ T_{k+} &= T_{k-} - m_k \Omega^2 (s_k - s_C)\, \gamma_0, \end{aligned} \tag{52}$$

and similarly to (20), the equilibrium tension can be expressed as

$$T_0(s) = \Omega_0^2 \gamma_0\, P(s), \tag{53}$$

where $P(s)$ is the solution of the boundary problem (21).

Within the linear elasticity region, the longitudinal stiffness of the tether can be related to its tension as

$$E(s) = \frac{T_0(s)}{\gamma_0 - 1} = k_E\, \Omega_0^2\, P(s), \qquad k_E = \frac{\gamma_0}{\gamma_0 - 1}. \tag{54}$$

With a strain on the order of $\gamma_0 - 1 \sim 0.01$, the coefficient $k_E \sim 100$.

The internal damping coefficient is usually considered directly proportional to the longitudinal stiffness and inversely proportional to the frequency of oscillations Ω_n, which gives

$$D(s, \Omega_n) = \frac{E(s)\,\eta}{\Omega_n} = \nu_n\, \Omega_0^2\, P(s), \qquad \nu_n = \frac{k_E \eta}{\Omega_n}, \tag{55}$$

where η is a loss factor, on the order of 0.1 for braided tethers.

After these substitutions, the first term under the integral in formula (50) takes the form

$$T_1 \mathbf{e}_1 = \Omega_0^2 P(s)\,[\gamma_0 + k_E\,(\gamma_1 - \gamma_*) + \nu_1\,\dot{\gamma}_1]\,\mathbf{e}_1 = \Omega_0^2 P(s)\, u_1\, \boldsymbol{\tau}_1,$$

where

$$u_1 = \frac{1}{\gamma_1}[\gamma_0 + k_E\,(\gamma_1 - \gamma_*) + \nu_1\,\dot{\gamma}_1], \tag{56}$$

and the expansion coefficients become

$$\mathbf{c}_n = \Omega_0^2 P(s)\,\left[k_E\, \mathbf{e}_1 q_{en} + \nu_n\, \mathbf{e}_1 \dot{q}_{en} + u_1\,(\mathbf{q}_n - \mathbf{e}_1 q_{en})\right].$$

If we assume that γ_* defined by (47) does not vary along the tether, *i.e.*, the creep rate, thermal expansion coefficient, and the temperature are the same for all tether elements, then we can apply the orthogonality condition (28) along with the eigenvalue relation (32) to derive

$$\mathbf{Q}_1 = -J_C\, \Omega_0^2\, u_1\, \boldsymbol{\tau}_1, \tag{57}$$

for $n = 1$ and

$$\mathbf{Q}_n = -||U_n||\,\beta_n^2 \Omega_0^2\,\left[k_E\, \mathbf{e}_1 q_{en} + \nu_n\, \mathbf{e}_1 \dot{q}_{en} + u_1\,(\mathbf{q}_n - \mathbf{e}_1 q_{en})\right] \tag{58}$$

for $n = 2, 3, \ldots$

Now, we can rewrite the equation of quasi-rigid rotation (42) as

$$\ddot{\boldsymbol{\tau}}_1 + \Omega_0^2\, u_1 \boldsymbol{\tau}_1 = \frac{1}{J_C}\,(\mathbf{G}_1 + \boldsymbol{\Phi}_1), \tag{59}$$

and the equations of tether oscillations (37), $n = 2, 3, \ldots$, as

$$\ddot{\mathbf{q}}_n + \beta_n^2 \Omega_0^2 \left[k_E \, \mathbf{e}_1 \, q_{en} + \nu_n \, \mathbf{e}_1 \, \dot{q}_{en} + u_1 \left(\mathbf{q}_n - \mathbf{e}_1 \, q_{en} \right) \right] = \frac{1}{||U_n||} \left(\mathbf{G}_n + \mathbf{\Phi}_n \right). \qquad (60)$$

7. GRAVITATIONAL FORCES

The gravitational terms in the equations of motion (41), (59) and (60) are defined by (39). The variation of the main component of the gravitational acceleration $\mathbf{g}$ along the tether can be represented in the linear approximation in displacement from the center of mass as

$$\mathbf{g} = -\frac{\mu_E \mathbf{R}}{R^3} \approx -\frac{\mu_E \mathbf{R}_C}{R_C^3} + \frac{\mu_E}{R_C^3} \left[3 \mathbf{e}_R \left(\mathbf{e}_R, \mathbf{r} \right) - \mathbf{r} \right], \qquad (61)$$

where μ_E is the gravity constant of the Earth, $\mathbf{e}_R = \mathbf{R}_C / R_C$ is a unit vector along the geocentric radius of the center of mass $\mathbf{R}_C$, and

$$\mathbf{r}(s,t) = (s - s_C) \, \boldsymbol{\tau}_1(t) + \sum_{n=2}^{\infty} \mathbf{q}_n(t) \, U_n(s) \qquad (62)$$

is the position vector relative to the center of mass.

Substituting expressions (61)–(62) into (39), and applying the orthogonality conditions (27) and the norm definition (29), we obtain

$$\begin{aligned} \mathbf{G}_0 &\approx -M \, \frac{\mu_E \mathbf{R}_C}{R_C^3}, \\ \mathbf{G}_1 &\approx J_C \, \frac{\mu_E}{R_C^3} \left[3 \mathbf{e}_R \left(\mathbf{e}_R, \boldsymbol{\tau}_1 \right) - \boldsymbol{\tau}_1 \right], \\ \mathbf{G}_n &\approx ||U_n|| \, \frac{\mu_E}{R_C^3} \left[3 \mathbf{e}_R \left(\mathbf{e}_R, \mathbf{q}_n \right) - \mathbf{q}_n \right], \quad n = 2, 3, \ldots, \end{aligned} \qquad (63)$$

where M is the total mass of the system (30), and J_C is the moment of inertia of an imaginary system with an unstretched straight tether about the center of mass defined by (31).

Note that in the linear approximation, the higher modes of oscillations do not affect the motion of the center of mass and the quasi-rigid rotation about the center of mass, and there is no practical need to include higher order terms in $\mathbf{q}_n$ as long as typical amplitudes of tether oscillations in a momentum exchange system are relatively small. However, to achieve the required precision, it is necessary to include higher order terms in $(s - s_C) \, \boldsymbol{\tau}_1$.

The variation of the main (Newtonian) term of the gravitational acceleration along the line $(s - s_C)\,\boldsymbol{\tau}_1$ drawn through the center of mass is given by

$$\mathbf{g} = -\frac{\mu_E \mathbf{R}}{R^3} = -\frac{\mu_E\,[\mathbf{R}_C + (s - s_C)\,\boldsymbol{\tau}_1]}{|\mathbf{R}_C + (s - s_C)\,\boldsymbol{\tau}_1|^3} = -\frac{\mu_E}{R_C^2}\,\frac{\mathbf{e}_R + \varepsilon \mathbf{e}_1}{(1 - 2x\varepsilon + \varepsilon^2)^{3/2}} \tag{64}$$

where

$$x = -(\mathbf{e}_R, \mathbf{e}_1), \qquad \mathbf{e}_1 = \frac{\boldsymbol{\tau}_1}{\gamma_1}, \qquad \varepsilon = \frac{(s - s_C)\,\gamma_1}{R_C}.$$

As known in the theory of Legendre functions,

$$\frac{1}{(1 - 2x\varepsilon + \varepsilon^2)^{1/2}} = \sum_{n=0}^{\infty} P_n(x)\,\varepsilon^n,$$

where $P_n(x)$ are Legendre polynomials. Differentiating this equation with respect to x and dividing by ε, we find that

$$\frac{1}{(1 - 2x\varepsilon + \varepsilon^2)^{3/2}} = \sum_{n=0}^{\infty} P'_{n+1}(x)\,\varepsilon^n,$$

where P'_n are the first derivatives of the Legendre polynomials.

After substituting this expression in (64), we obtain

$$\mathbf{g} = -\frac{\mu_E}{R_C^2} \sum_{n=0}^{\infty} \left[\mathbf{e}_R\,P'_{n+1}(x) + \mathbf{e}_1\,P'_n(x)\right] \left[\frac{(s - s_C)\,\gamma_1}{R_C}\right]^n. \tag{65}$$

This series expansion converges rapidly because $(s - s_C)/R_C$ is typically small, on the order of 0.01. To determine a minimum number of terms required for practical computation, consider a simple inequality

$$n \left(\frac{L}{R_C}\right)^n \lesssim \delta, \qquad \text{or} \qquad n \gtrsim \frac{\ln(n/\delta)}{\ln(R_C/L)}, \tag{66}$$

where the left part estimates the contribution of the n-th term, L is the total tether length, and δ is a maximum acceptable relative error. Generally, all terms $n \geqslant N$, where N is the minimum number satisfying (66), can be dropped. For a typical momentum exchange system, it is sufficient to retain only 5 terms at the perigee, and 4 terms at the apogee to achieve 10-digit precision ($\delta \sim 10^{-10}$).

Expansion (65) can be also presented as

$$\mathbf{g} = \sum_{n=0}^{\infty} \mathbf{g}_C^n\,(s - s_C)^n, \qquad \mathbf{g}_C^n = \frac{1}{n!}\,\frac{\partial^n \mathbf{g}}{\partial\, s^n}\bigg|_C, \tag{67}$$

where the derivatives with respect to s are calculated along the line $(s - s_C)\,\tau_1$ drawn through the center of mass. For the Newtonian term, according to (65),

$$\mathbf{g}_C^n = -\frac{\mu_E\,\gamma_1^n}{R_C^{2+n}}\,\left[\mathbf{e}_R\,P'_{n+1}(x) + \mathbf{e}_1\,P'_n(x)\right] \tag{68}$$

Note that expansion (67) can be treated more broadly to include all terms of the standard representation of the Earth gravitational field, as well as the gravitational fields of other celestial bodies.

Using (67), the generalized gravitational forces $\mathbf{G}_n$ (39) can be represented as

$$\mathbf{G}_n = \sum_{k=0}^{\infty} \mathbf{g}_C^k\,I_n^k, \qquad I_n^k = \langle (s - s_C)^k,\, U_n \rangle. \tag{69}$$

Applying the orthogonality conditions (27), norm definition (29), and trivial form properties (24)–(25), (30)–(31), we find that

$$\begin{array}{llllll} I_0^0 = M, & I_0^1 = 0, & I_0^2 = J_C, & \ldots & I_0^k = I_k, & \ldots \\ I_1^0 = 0, & I_1^1 = J_C, & I_0^2 = I_3, & \ldots & I_1^k = I_{k+1}, & \ldots \end{array} \tag{70}$$

where I_n are the high order moments,

$$I_n = m_A\,(s_A - s_C)^n + m_B\,(s_B - s_C)^n + \sum_k m_k\,(s_k - s_C)^n + \int_A^B \rho\,(s - s_C)^n ds. \tag{71}$$

We note also that

$$I_n^0 = I_n^1 = 0, \qquad n = 2, 3, \ldots \tag{72}$$

The practical benefit of using expansion (69) is that the quantities I_n^k can be precomputed to avoid integration of the gravitational force along the tether on each step of solution propagation.

Another practical question is to estimate how many terms of the gravitational field expansion (5) must be retained to achieve the required accuracy. The problem is in the slow convergence of the series expansion at low altitudes when the ratio R_E/R is close to 1.

On average, according to the Kaula rule [7], the normalized geopotential coefficients $\bar{C}_{nm}$ and $\bar{S}_{nm}$ decrease in inverse proportion to the second power of their degree,

$$\bar{C}_{nm}, \bar{S}_{nm} \sim \frac{10^{-5}}{n^2}. \tag{73}$$

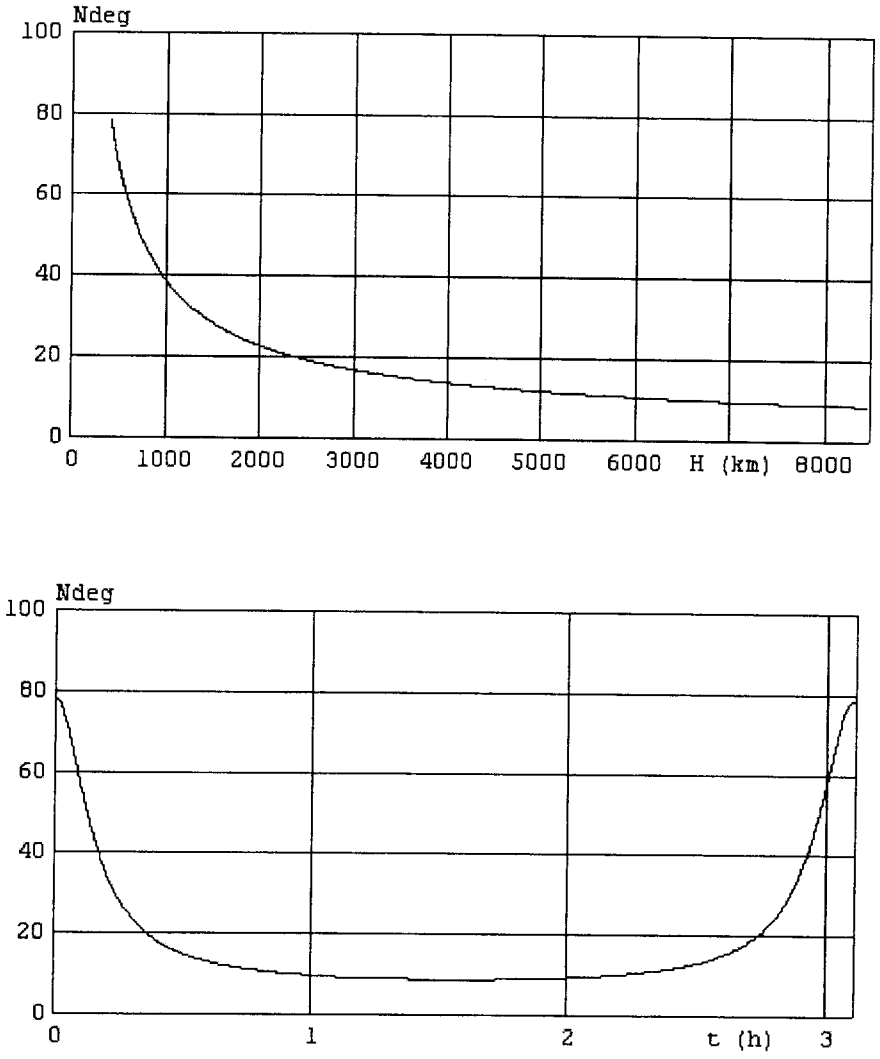

Fig. 6. Minimum degree of the geopotential expansion for MXER.

Taking this empirical rule into account, the following inequality roughly estimates the contribution of the higher degree terms to the acceleration of the center of mass of a momentum exchange tether system,

$$\frac{10^{-5}}{n}\left(\frac{R_E}{R_C}\right)^n \lesssim \delta, \qquad \text{or} \qquad n \gtrsim \frac{\ln\left(n\,\delta \cdot 10^5\right)}{\ln\left(R_C/R_E\right)}. \tag{74}$$

Numerical experiments show that a value of $\delta \sim 10^{-9}$ can be assumed for MXER to achieve better than 1 m prediction accuracy over one orbit. The minimum degree N that satisfies (74) is shown in Fig. 6 as a function of the geocentric radius and flight time. We see that a lower degree model is adequate for the most part of the orbit, but a model of a much higher degree is needed during perigee passages.

8. SIMULATION APPROACH

Now, we can gather all equations, and apply formulas for the gravitational forces derived in the previous section. The equation of motion of the center of mass (41) takes the form

$$\ddot{\mathbf{R}}_C = \mathbf{g}_C^0 + \frac{1}{M} \sum_{k=2}^{\infty} \mathbf{g}_C^k I_0^k + \frac{\mathbf{\Phi}_0}{M}, \tag{75}$$

the equation of the quasi-rigid rotation (59) can be rewritten as

$$\ddot{\tau}_1 + \Omega_0^2 u_1 \tau_1 = \mathbf{g}_C^1 + \frac{1}{J_C} \sum_{k=2}^{\infty} \mathbf{g}_C^k I_1^k + \frac{\mathbf{\Phi}_1}{J_C}, \tag{76}$$

and the equations of tether oscillation (37), $n = 2, 3, \ldots$, can be reduced to

$$\begin{aligned} \ddot{\mathbf{q}}_n + \beta_n^2 \Omega_0^2 \left[k_E \, \mathbf{e}_1 q_{en} + \nu_n \, \mathbf{e}_1 \dot{q}_{en} + u_1 \left(\mathbf{q}_n - \mathbf{e}_1 q_{en} \right) \right] = \\ \frac{\mu_E}{R_C^3} \left[3 \mathbf{e}_R \left(\mathbf{e}_R, \mathbf{q}_n \right) - \mathbf{q}_n \right] + \frac{1}{||U_n||} \sum_{k=2}^{\infty} \mathbf{g}_C^k I_n^k + \frac{\mathbf{\Phi}_n}{||U_n||}. \end{aligned} \tag{77}$$

As noted earlier, very few terms $\mathbf{g}_C^k$ are needed to achieve the desired precision, and quantities I_n^k can be precomputed.

Equations (75)–(77) cleanly separate three dynamically different kinds of motions of the momentum exchange tether system. They are compact and flexible in sense that the number of the gravitational terms and the number of the tether oscillation modes can be selected depending on the desired accuracy. This opens a way to building a very computationally effective simulator.

Preliminary testing for a typical momentum exchange system showed that equations (75)–(77) can be integrated with a time step of about 4 seconds of orbital time, and it takes only a few seconds on a standard issue PC to propagate a solution over one orbit with 9–10 digit precision. More studies are needed to understand possible limitations of this approach.

REFERENCES

1. MORAVEC, H., A Non-Synchronous Orbital Skyhook, *Journal of the Astronautical Sciences,* **25(4),** Oct-Dec 1977, pp. 307-322.

2. HOYT, R., UPHOFF, C., Cislunar Tether Transport System, AIAA 99-2690, 1999

3. HOYT, R., Design and Simulation of a Tether Boost Facility for The HASTOL Architecture, AIAA Paper 2000-3615, 36th Joint Propulsion Conference, July 2000.

4. SORENSEN, K.F., Conceptual Design and Analysis of an MXER Tether Boost Station, AIAA 2001-3915, 2001

5. BELETSKY, V.V. AND LEVIN, E.M. Dynamics of Space Tether Systems. *Advances in the Astronautical Sciences,* AAS, **83,** 1993, Univelt, Inc.

6. LEMOINE, F.G., KENYON, S.C., FACTOR, J.K., TRIMMER, R.G., PAVLIS, N.K., CHINN, D.S., COX, C.M., KLOSKO, S.M., LUTHCKE, S.B., TORRENCE, M.H., WANG, Y.M., WILLIAMSON, R.G., PAVLIS, E.C., RAPP, R.H. AND OLSON, T.R. The Development of the Joint NASA GSFC and NIMA Geopotential Model EGM96, NASA Goddard Space Flight Center, NASA TP-1998-206891, July 1998.

7. MONTENBRUCK, O. AND GILL, E. *Satellite Orbits: Models, Methods and Applications,* Springer Verlag, 2000.

APPENDIX B—MXER SIMULATION STUDY, PART II

STAR, Inc.

MXER SIMULATION STUDY

E. M. LEVIN

Part II

Prepared for MSFC
November 17, 2005

Typeset by AMS-TEX

NOMENCLATURE

A = first end-body
B = second end-body
C = center of mass of the tether system
E = longitudinal stiffness of the tether
$\mathbf{F}$ = non-gravitational forces
$\mathbf{g}$ = gravitational acceleration
J_C = moment of inertia of the tether system
L = total tether length
L_k = length of the k-th segment of the tether
m_A = mass of the first end-body
m_B = mass of the second end-body
m_k = embedded mass k
M = total mass of the tether system
$\mathbf{R}$ = geocentric radius-vector
R_E = mean radius of the Earth
R_C = geocentric radius of the center of mass
s = arclength along the unstretched tether
T = tether tension
$\mathbf{T}$ = tether tension vector
t = time
γ = tether elongation
ρ = tether mass per unit length
$\boldsymbol{\tau}$ = unit vector along the tether line
$\boldsymbol{\tau}_1$ = direction of the imaginary straight tether line
Ω = rotational angular rate
$(\dot{})$ = differentiation with respect to time
$(')$ = differentiation with respect to the arclength
$(\mathbf{a}, \mathbf{b})$ = scalar product of vectors $\mathbf{a}$ and $\mathbf{b}$

1. EQUATIONS OF MOTION IN NEWTONIAN FORM

In the first part of this study [1], we considered the dynamics of a momentum exchange system consisting of two end-bodies and a number of power stations connected with tether segments. The end-bodies A and B and the power stations k were modeled as point masses m_A, m_B, and m_k, respectively. The power stations are connected with tether segments of lengths L_k, as shown in Fig. 1. The tether segment L_k connects masses m_k and m_{k+1}.

Fig. 1. Structure of the momentum exchange tether system.

All point masses and the masses of the tether segments are assumed to be constant. Tether mass per unit length can vary along the tether.

Positions of the tether elements with respect to a non-rotating geocentric reference frame $OXYZ$ are defined by the geocentric radius $\mathbf{R}$ as a function of the arclength s measured along the unstretched tether from A to B, and time t,

$$\mathbf{R} = \mathbf{R}(s,t),$$

Positions of the end masses and embedded masses are

$$\mathbf{R}_A = \mathbf{R}(s_A,t), \quad \mathbf{R}_B = \mathbf{R}(s_B,t), \quad \mathbf{R}_k = \mathbf{R}(s_k,t).$$

The tension vector $\mathbf{T}$ of a perfectly flexible tether is tangent to the tether line,

$$\mathbf{T} = T\boldsymbol{\tau}, \qquad \boldsymbol{\tau} = \frac{\mathbf{R}'}{\gamma}, \qquad \gamma = |\mathbf{R}'|, \tag{1}$$

where $\boldsymbol{\tau}$ is a unit vector tangent to the tether line, prime denotes differentiation with respect to the arclength s, and γ is the local tether elongation.

The tether tension T can be expressed as a function of the elongation γ, elongation rate $\dot{\gamma}$, temperature Θ, and other factors,

$$T = T(s,\, t,\, \gamma,\, \dot{\gamma},\, \Theta, \ldots). \tag{2}$$

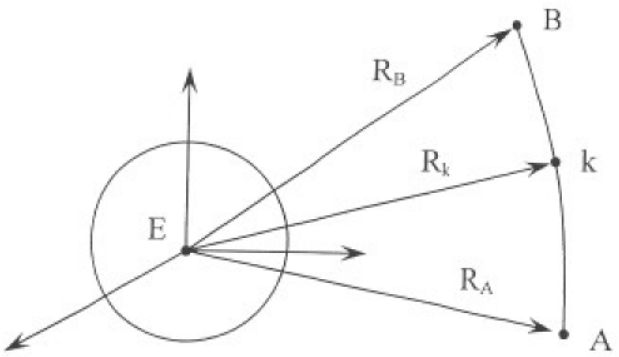

Fig. 2. Positions of the tether system elements.

Equations of motion of the tether system derived in [1] include ordinary and partial differential equations. The motion of the end masses and embedded masses is described by the ordinary differential equations

$$\begin{aligned} m_A \ddot{\mathbf{R}}_A &= \mathbf{T}_A + m_A \mathbf{g}_A + \mathbf{F}_A \\ m_B \ddot{\mathbf{R}}_B &= -\mathbf{T}_B + m_B \mathbf{g}_B + \mathbf{F}_B \\ m_k \ddot{\mathbf{R}}_k &= \mathbf{T}_{k+} - \mathbf{T}_{k-} + m_k \mathbf{g}_k + \mathbf{F}_k \end{aligned} \tag{3}$$

where dots denote differentiation with respect to time, $\mathbf{g}_A$, $\mathbf{g}_B$, and $\mathbf{g}_k$ are the gravity accelerations at points A, B, and k, respectively, while $\mathbf{F}_A$, $\mathbf{F}_B$, and $\mathbf{F}_k$ are non-gravitational forces acting on the end masses and embedded masses. The tether tension vectors are taken at the following points: $\mathbf{T}_A$ at point A, $\mathbf{T}_B$ at point B, $\mathbf{T}_{k-}$ at point k of segment L_{k-1}, and $\mathbf{T}_{k+}$ at point k of segment L_k.

The motion of the tether is described by the partial differential equation

$$\rho \ddot{\mathbf{R}} = \mathbf{T}' + \rho \mathbf{g} + \mathbf{F} \tag{4}$$

where dots denote differentiation with respect to time t, and primes denote differentiation with respect to the arclength s, ρ is the tether mass per unit length, and $\mathbf{T}$ is the tether tension.

In the general case, the tether mass per unit length ρ can vary along the tether, but we will concentrate on a more practical case when ρ is constant along each tether segment connecting the end masses,

$$\rho = \rho_k, \qquad k = 1, \ldots, K. \tag{5}$$

2. EQUATIONS OF MOTION IN MINAKOV'S FORM

Equations of motion in Minakov's form, introduced into space tether dynamics in [2], are obtained as follows. First, we differentiate equation (4) with respect to the arclength s,

$$\rho\,\ddot{\mathbf{R}}' = \mathbf{T}'' + \rho\,\mathbf{g}' + \mathbf{F}'.$$

Keeping in mind that $\mathbf{R}' = \gamma\tau$ and $\mathbf{T} = T\tau$, we find that

$$\rho\,(\ddot{\gamma}\tau + 2\dot{\gamma}\dot{\tau} + \gamma\ddot{\tau}) = T''\tau + 2T'\tau' + T\tau'' + \rho\,\mathbf{g}' + \mathbf{F}'. \tag{6}$$

By definition, the unit tangent vector τ satisfies the condition

$$(\tau,\tau) = 1. \tag{7}$$

The first differentiation with respect to the arclength and time yields two orthogonality conditions,

$$(\tau,\dot{\tau}) = 0, \qquad (\tau,\tau') = 0, \tag{8}$$

while the second differentiation yields two kinematic relations,

$$(\tau,\ddot{\tau}) = -(\dot{\tau},\dot{\tau}), \qquad (\tau,\tau'') = -(\tau',\tau'). \tag{9}$$

Multiplying equation (6) by vector τ (scalar product) and taking into account relations (7)–(9), we obtain a scalar equation of the second order with respect to tension,

$$\rho\,\ddot{\gamma} - \rho\gamma\,(\dot{\tau},\dot{\tau}) = T'' - T\,(\tau',\tau') + \rho\,(\mathbf{g}',\tau) + (\mathbf{F}',\tau). \tag{10}$$

From this equation, we express the second derivative of tension as

$$T'' = T\,(\tau',\tau') + \rho\,\ddot{\gamma} - \rho\gamma\,(\dot{\tau},\dot{\tau}) - \rho\,(\mathbf{g}',\tau) - (\mathbf{F}',\tau). \tag{11}$$

Substituting expression (11) into equation (6), we arrive at the following equation of the second order with respect to the unit tangent vector τ,

$$\rho\,[\gamma\ddot{\tau} + 2\dot{\gamma}\dot{\tau} + \gamma\tau\,(\dot{\tau},\dot{\tau})] = T\,[\tau'' + (\tau',\tau')\,\tau] + 2T'\tau' + \rho\mathbf{g}' + \mathbf{F}' - (\rho\mathbf{g}' + \mathbf{F}',\tau)\,\tau. \tag{12}$$

This equation describes transverse motion of the tether and it has an obvious wave structure with a transverse wave velocity equal to

$$v_t = \sqrt{\frac{T}{\rho\gamma}}. \tag{13}$$

Equation (10) describes longitudinal motion of the tether and it also has a wave structure. To reveal this structure, we consider a case of linear elasticity,

$$T = T_0 + E(\gamma - \gamma_*), \tag{14}$$

where T_0 is a reference tension, E is the tether longitudinal stiffness, and γ_* is the equilibrium elongation under the reference tension T_0. According to (14), and keeping in mind that γ_* may vary with time and temperature, we have

$$\ddot{\gamma} = \frac{\ddot{T}}{E} + \ddot{\gamma}_*.$$

After substituting this relation into equation (10), we can clearly see that this equation has a wave structure with a longitudinal wave velocity equal to

$$v_e = \sqrt{\frac{E}{\rho}}. \tag{15}$$

The longitudinal wave velocity (15) is much higher than the transverse wave velocity (13), and therefore, the system of equations (10) and (12) is stiff in the sense that equation (12) describes high frequency longitudinal oscillations, while equation (10) describes transverse oscillations of much lower frequencies. The advantage of Minakov's form of the equations lies in the separation of the high and low frequency wave structures in the tether dynamics equations.

In the Newtonian field,

$$\mathbf{g} = -\frac{\mu_E \mathbf{R}}{R^3},$$

the gravity gradient along the tether is calculated as

$$\mathbf{g}' = -\frac{\mu_E \mathbf{R}'}{R^3} + \frac{3\mu_E \mathbf{R}}{R^5}(\mathbf{R}, \mathbf{R}') = \frac{\mu_E \gamma}{R^3}[3\mathbf{e}_R(\mathbf{e}_R, \boldsymbol{\tau}) - \boldsymbol{\tau}], \tag{16}$$

where μ_E is the gravitational constant of the Earth, $\mathbf{e}_R = \mathbf{R}/R$ is a unit vector along the geocentric radius vector $\mathbf{R}$, and $\mathbf{R}' = \gamma\boldsymbol{\tau}$. The corresponding gravitational term in the equation of longitudinal motion (10) is reduced to

$$(\mathbf{g}', \boldsymbol{\tau}) = \frac{\mu_E \gamma}{R^3}[3(\mathbf{e}_R, \boldsymbol{\tau})^2 - 1], \tag{17}$$

while the respective gravitational term in the equation of transverse motion (12) takes the form

$$\mathbf{g}' - (\mathbf{g}', \boldsymbol{\tau})\boldsymbol{\tau} = \frac{\mu_E \gamma}{R^3} 3(\mathbf{e}_R, \boldsymbol{\tau})[\mathbf{e}_R - (\mathbf{e}_R, \boldsymbol{\tau})\boldsymbol{\tau}]. \tag{18}$$

3. BOUNDARY CONDITIONS

The equations of tether motion must be complemented with boundary conditions at the ends of each tether segment. To derive these boundary conditions, we express the accelerations of the end masses A and B and the embedded masses m_k from equation (3)

$$\ddot{\mathbf{R}}_A = \frac{\mathbf{T}_A + \mathbf{F}_A}{m_A} + \mathbf{g}_A,$$
$$\ddot{\mathbf{R}}_B = \frac{-\mathbf{T}_B + \mathbf{F}_B}{m_B} + \mathbf{g}_B,$$
$$\ddot{\mathbf{R}}_k = \frac{\mathbf{T}_{k+} - \mathbf{T}_{k-} + \mathbf{F}_k}{m_k} + \mathbf{g}_k,$$

and from equation (4) at the ends of the tether segments,

$$\ddot{\mathbf{R}}_A = \left(\frac{\mathbf{T}' + \mathbf{F}}{\rho}\right)_A + \mathbf{g}_A,$$
$$\ddot{\mathbf{R}}_B = \left(\frac{\mathbf{T}' + \mathbf{F}}{\rho}\right)_B + \mathbf{g}_B,$$
$$\ddot{\mathbf{R}}_k = \left(\frac{\mathbf{T}' + \mathbf{F}}{\rho}\right)_{k+} + \mathbf{g}_k = \left(\frac{\mathbf{T}' + \mathbf{F}}{\rho}\right)_{k-} + \mathbf{g}_k.$$

This yields the following boundary conditions

$$\begin{aligned} \mathbf{T}'|_A &= \mathbf{Q}_A, & \mathbf{T}'|_B &= \mathbf{Q}_B, \\ \mathbf{T}'|_{k-} &= \mathbf{Q}_{k-}, & \mathbf{T}'|_{k+} &= \mathbf{Q}_{k+}, \end{aligned} \tag{19}$$

where

$$\begin{aligned} \mathbf{Q}_A &= \frac{\rho_A}{m_A}(\mathbf{T}_A + \mathbf{F}_A) - \mathbf{F}|_A, \\ \mathbf{Q}_B &= \frac{\rho_B}{m_B}(-\mathbf{T}_B + \mathbf{F}_B) - \mathbf{F}|_B, \\ \mathbf{Q}_{k-} &= \frac{\rho_{k-}}{m_k}(\mathbf{T}_{k+} - \mathbf{T}_{k-} + \mathbf{F}_k) - \mathbf{F}|_{k-}, \\ \mathbf{Q}_{k+} &= \frac{\rho_{k+}}{m_k}(\mathbf{T}_{k+} - \mathbf{T}_{k-} + \mathbf{F}_k) - \mathbf{F}|_{k+}. \end{aligned} \tag{20}$$

Note that the gravitational accelerations canceled out and are not included in the boundary conditions.

Keeping in mind that $\mathbf{T}' = T'\boldsymbol{\tau} + T\boldsymbol{\tau}'$, according to (1), we multiply each of the relations (19) by the corresponding unit tangent vector $\boldsymbol{\tau}$ (scalar product) and arrive at the following conditions

$$\begin{aligned} T'|_A &= (\mathbf{Q}_A, \boldsymbol{\tau}_A), & T'|_B &= (\mathbf{Q}_B, \boldsymbol{\tau}_B), \\ T'|_{k-} &= (\mathbf{Q}_{k-}, \boldsymbol{\tau}_{k-}), & T'|_{k+} &= (\mathbf{Q}_{k+}, \boldsymbol{\tau}_{k+}), \end{aligned} \tag{21}$$

Relations (21) serve as boundary conditions for equation (10) describing longitudinal motion of the tether.

Substituting relations (21) into (19), we find boundary conditions for equation (12) describing transverse motion of the tether,

$$\begin{aligned} \boldsymbol{\tau}'|_A &= \frac{1}{T_A}\left[\mathbf{Q}_A - (\mathbf{Q}_A, \boldsymbol{\tau}_A)\,\boldsymbol{\tau}_A\right], \\ \boldsymbol{\tau}'|_B &= \frac{1}{T_B}\left[\mathbf{Q}_B - (\mathbf{Q}_B, \boldsymbol{\tau}_B)\,\boldsymbol{\tau}_B\right], \\ \boldsymbol{\tau}'|_{k-} &= \frac{1}{T_{k-}}\left[\mathbf{Q}_{k-} - (\mathbf{Q}_{k-}, \boldsymbol{\tau}_{k-})\,\boldsymbol{\tau}_{k-}\right], \\ \boldsymbol{\tau}'|_{k+} &= \frac{1}{T_{k+}}\left[\mathbf{Q}_{k+} - (\mathbf{Q}_{k+}, \boldsymbol{\tau}_{k+})\,\boldsymbol{\tau}_{k+}\right]. \end{aligned} \tag{22}$$

The boundary conditions are simplified when the non-gravitational forces $\mathbf{F}$ are neglected. The boundary conditions for the transverse motion of the tether are reduced to

$$\begin{aligned} \boldsymbol{\tau}'|_A &= \mathbf{0}, \\ \boldsymbol{\tau}'|_B &= \mathbf{0}, \\ \boldsymbol{\tau}'|_{k-} &= \frac{\rho_{k-}}{m_k}\,\frac{T_{k+}}{T_{k-}}\,(\boldsymbol{\tau}_{k+} - \varkappa_k \boldsymbol{\tau}_{k-}), \\ \boldsymbol{\tau}'|_{k+} &= \frac{\rho_{k+}}{m_k}\,\frac{T_{k-}}{T_{k+}}\,(\varkappa_k \boldsymbol{\tau}_{k+} - \boldsymbol{\tau}_{k-}), \end{aligned} \tag{23}$$

where

$$\varkappa_k = (\boldsymbol{\tau}_{k+}, \boldsymbol{\tau}_{k-}),$$

while the boundary conditions for the longitudinal motion of the tether take the form

$$\begin{aligned} T'|_A &= \frac{\rho_A}{m_A}\,T_A, & T'|_B &= -\frac{\rho_B}{m_B}\,T_B, \\ T'|_{k-} &= \frac{\rho_{k-}}{m_k}\,(\varkappa_k T_{k+} - T_{k-}), & T'|_{k+} &= \frac{\rho_{k+}}{m_k}\,(T_{k+} - \varkappa_k T_{k-}). \end{aligned} \tag{24}$$

4. MOTION OF THE CENTER OF MASS

The equations of tether motion derived in the previous sections describe evolution of the tether orientation and shape. They must be solved together with one of the ordinary differential equations (3) describing the orbital motion of one of the end masses or embedded masses, or with the equation of motion of the center of mass

$$\ddot{\mathbf{R}}_C = \frac{1}{M}(\mathbf{G}_0 + \mathbf{\Phi}_0), \tag{25}$$

where $\mathbf{R}_C$ is the geocentric radius vector of the center of mass, M is the total mass of the tether system, $\mathbf{G}_0$ is the sum of the gravitational forces

$$\mathbf{G}_0 = m_A\mathbf{g}_A + m_B\mathbf{g}_B + \sum_k m_k\mathbf{g}_k + \int_A^B \rho\mathbf{g}\,ds, \tag{26}$$

and $\mathbf{\Phi}_0$ is the sum of the non-gravitational forces acting on the tether system,

$$\mathbf{\Phi}_0 = \mathbf{F}_A + \mathbf{F}_B + \sum_k \mathbf{F}_k + \int_A^B \mathbf{F}\,ds. \tag{27}$$

As shown in the first part of this report [1], the sum of the gravitational forces can be represented as a series

$$\mathbf{G}_0 = M\mathbf{g}_C^0 + \sum_{n=2}^{\infty} \mathbf{g}_C^n I_n + \frac{\mathbf{\Phi}_0}{M}, \tag{28}$$

where $\mathbf{g}_C^0$ is the gravitational acceleration at the center of mass, $\mathbf{g}_C^n$ are derivatives of the gravitational acceleration along the "mean" tether line $\mathbf{R} = \mathbf{R}_C + (s - s_C)\,\tau_1$ drawn through the center of mass,

$$\mathbf{g}_C^n = \frac{1}{n!}\left.\frac{\partial^n \mathbf{g}}{\partial s^n}\right|_C,$$

and quantities I_n represent the high order moments

$$I_n = m_A(s_A - s_C)^n + m_B(s_B - s_C)^n + \sum_k m_k(s_k - s_C)^n + \int_A^B \rho(s - s_C)^n ds.$$

The direction of the "mean" tether line τ_1 is defined as follows. As shown in the first part of this report [1], the tether shape can be represented by the series

$$\mathbf{R}(s,t) = \mathbf{R}_C(t) + (s - s_C)\,\tau_1(t) + \sum_{n=2}^{\infty} \mathbf{q}_n(t)\,U_n(s), \tag{29}$$

where $\mathbf{q}_n(t)$ are generalized coordinates and $U_n(s)$ are the eigenforms of tether oscillations. Differentiating this equation with respect to the arclength, and keeping in mind that $\mathbf{R}' = \gamma\tau$, we derive

$$\tau_1 = \gamma\tau - \sum_{n=2}^{\infty} \mathbf{q}_n(t)\,U_n'(s). \tag{30}$$

The orthogonality conditions for the eigenforms can be expressed as

$$\int_A^B P\,U_i'U_j'\,ds = 0, \qquad i \neq j, \tag{31}$$

where $P = P(s)$ represents a normalized tension profile, defined as the solution to the following boundary problem [1],

$$\begin{aligned} P' &= -\rho\,(s - s_C), \\ P_A &= -m_A(s_A - s_C), \\ P_B &= m_B(s_B - s_C), \\ P_{k+} &= P_{k-} - m_k(s_k - s_C), \end{aligned} \tag{32}$$

The first eigenform describes the rigid rotation $U_1 = s - s_C$, for which $U_1' = 1$. Multiplying equation (30) by $PU_1' = P$, integrating over the entire tether length, and applying the orthogonality conditions (31), we find that

$$\tau_1 \int_A^B P\,ds = \int_A^B P\gamma\tau\,ds. \tag{33}$$

The integral of P, according to [1], is equal to the moment of inertia of the undeformed tether system about the center of mass

$$\begin{aligned} &\int_A^B P\,ds = ||U_1|| = J_C = \\ &m_A\,(s_A - s_C)^2 + m_B\,(s_B - s_C)^2 + \sum_k m_k\,(s_k - s_C)^2 + \int_A^B \rho\,(s - s_C)^2\,ds, \end{aligned} \tag{34}$$

and therefore, relation (33) can be rewritten as

$$\tau_1 = \frac{1}{J_C} \int_A^B P\gamma\tau \, ds. \tag{35}$$

Formula (35) defines the "mean" tether direction for any given tether shape under the assumptions of the current formulation.

Knowing τ_1, we can calculate derivatives (26). As shown in [1], the Newtonian term of the gravitational field gives

$$\mathbf{g}_C^n = -\frac{\mu_E \gamma_1^n}{R_C^{2+n}} \left[\mathbf{e}_R P'_{n+1}(x) + \mathbf{e}_1 P'_n(x) \right] \tag{36}$$

where $\mathbf{e}_R = \mathbf{R}_C/|\mathbf{R}_C|$ is the unit vector of the geocentric direction to the center of mass, $\gamma_1 = |\tau_1|$, $\mathbf{e}_1 = \tau_1/\gamma_1$, $P_n(x)$ are Legendre polynomials, and $x = -(\mathbf{e}_R, \mathbf{e}_1)$.

To close the system of equations, we need to find the geocentric positions of all elements of the tether system. For a given tether shape, we know the relative positions $\mathbf{r} = \mathbf{R} - \mathbf{R}_A$ of all elements, and from the definition of the center of mass, we can find its relative position

$$\mathbf{r}_C = \frac{1}{M}\Big(m_B \mathbf{r}_B + \sum_k m_k \mathbf{r}_k + \int_A^B \rho \, \mathbf{r} \, ds \Big). \tag{37}$$

Using this information, we can calculate the geocentric position of the end point $\mathbf{R}_A = \mathbf{R}_C - \mathbf{r}_C$ and the geocentric positions of all other points of the tether system $\mathbf{R} = \mathbf{R}_A + \mathbf{r}$.

5. QUASI-STATIC TENSION

The longitudinal oscillations of the tether system are directly affected by the internal friction in the tether, while the transverse oscillations are are affected indirectly, through a weak coupling with the longitudinal oscillations.

As discussed in [2], one way to model internal friction in the tether is to add a term $\rho\chi\dot{\gamma}$, where χ is an effective damping coefficient, to the left side of the equation of longitudinal motion (10). It is shown in [2] that the energy dissipation in the tether can rapidly damp out high frequency longitudinal oscillations, and after a short period of time the longitudinal motion becomes quasi-static. Tension variations in the quasi-static motion are induced by relatively slow transverse motions and can be described by equation (11) without the term $\rho\ddot{\gamma}$,

$$T'' = T(\tau', \tau') - \rho\gamma(\dot{\tau}, \dot{\tau}) - \rho(\mathbf{g}', \tau) - (\mathbf{F}', \tau). \tag{38}$$

At any given moment t, this equation can be treated as an ordinary differential equation with respect to the tether tension T. Along with the boundary conditions (21), it defines the tether tension profile as a function of the dynamic state of the tether, including the tether shape, elongation and the angular rate distribution along the tether.

Similar to (24), the boundary conditions (21) can be presented as

$$\begin{aligned} T'|_A &= \frac{\rho_A}{m_A} T_A + f_A, \\ T'|_B &= -\frac{\rho_B}{m_B} T_B + f_B, \\ T'|_{k-} &= \frac{\rho_{k-}}{m_k} (\varkappa_k T_{k+} - T_{k-}) + f_{k-}, \\ T'|_{k+} &= \frac{\rho_{k+}}{m_k} (T_{k+} - \varkappa_k T_{k-}) + f_{k+}, \end{aligned} \tag{39}$$

where

$$\begin{aligned} f_A &= \frac{\rho_A}{m_A} (\mathbf{F}_A, \tau_A) - (\mathbf{F}|_A, \tau_A), \\ f_B &= \frac{\rho_B}{m_B} (\mathbf{F}_B, \tau_B) - (\mathbf{F}|_B, \tau_B), \\ f_{k-} &= \frac{\rho_{k-}}{m_{k-}} (\mathbf{F}_k, \tau_{k-}) - (\mathbf{F}|_{k-}, \tau_{k-}), \\ f_{k+} &= \frac{\rho_{k+}}{m_{k+}} (\mathbf{F}_k, \tau_{k+}) - (\mathbf{F}|_{k+}, \tau_{k+}). \end{aligned}$$

As we see in relation (16), the gravity gradient $\mathbf{g}'$ calculated along the tether is proportional to the elongation γ, $\mathbf{g}' = \gamma \mathbf{g}'_0$. This is true for any gravitational field, not only Newtonian. Also, it has been shown in [2] that the aerodynamic and Ampere forces, as well as solar radiation pressure acting on a tether element are proportional to the elongation, $\mathbf{F} = \gamma \mathbf{F}_0$. Formally, the gradient of these forces $\mathbf{F}'$ will include quadratic terms in γ because of the variation of the environmental parameters along the tether, however, these terms can be linearized with respect to small variations of elongation.

Under these assumptions, if we use the linear elasticity relation (14) between the elongation and tension, then we will have

$$\gamma = \gamma_* + (T - T_0)/E, \tag{40}$$

and equation (38) will be linear with respect to T. The boundary conditions (39) will also be linear with respect to T.

The general solution of the linear boundary problem (38)–(39) at any given moment t can be represented as a sum of two solutions,

$$T(s,t) = T_0(s,t) + c_1 T_1(s,t). \tag{41}$$

Solution T_0 is obtained as follows. We set T_{0A} to zero and determine T'_{0A} from the first equation of the system (39),

$$T_{0A} = 0, \qquad T'_{0A} = f_A. \tag{42}$$

Then, we integrate equation (38) with the initial conditions (42) over the first tether segment and find T_{k-} and T'_{k-} at the end of the segment. Now, we use the third equation of the system (39) to find the tension at the beginning of the next tether segment

$$T_{k+} = \frac{1}{\varkappa_k}\left[T_{k-} + \frac{m_k}{\rho_{k-}}(T'_{k-} - f_{k-})\right]. \tag{43}$$

We then substitute quantity (43) into the last equation of the system (39) to find the derivative T'_{k+} at the beginning of the next segment.

This process is repeated until we arrive at the end B and determine the values of T_{0B} and T'_{0B}. Generally, these values will not satisfy the second equation of the system (39). We need solution T_1 to match the boundary condition at the end B.

Solution T_1 is calculated as follows. We introduce a new system of equations (38′)–(39′) which retains only terms linear in T from the original equations (38)–(39). We set T_{1A} to some reference tension T_*,

$$T_{1A} = T_*, \tag{44}$$

find T'_{1A} from the first equation of the homogeneous system (39′), and integrate the homogeneous equation (38′) over the first tether segment. We then use the third and the last equation of system (39′) to find T_{k+} and T'_{k+} at the beginning of the next segment, and continue integration until we reach the end B.

Now, we can substitute the general form of solution (41) into the second equation of (39) and find the coefficient c_1 from the following equation

$$T'_{0B} + \frac{\rho_B}{m_B}T_{0B} + c_1\left(T'_{1B} + \frac{\rho_B}{m_B}T_{1B}\right) = f_B. \tag{45}$$

One of the major benefits of this approach is that we reduced the initially stiff system of equations (10), (12) to a non-stiff system (12), (38) by abstracting from the fast transient processes in longitudinal oscillations. This does not mean that we neglected tether elongation, we only filtered out its high frequency components.

6. SIMULATION APPROACH

For a numerical solution, equations (12), (22), (38), (39) can be discretized with respect to the arclength s. This will reduce the partial differential equation

(12) to a set of ordinary differential equations at the discretization nodes. These equations are complemented with the ordinary differential equation (25) describing the motion of the center of mass.

The number of discretization nodes is determined by the required accuracy. To get an idea of a typical number of nodes, let us consider a very simple model of a string clamped at the ends A and B. Its transverse oscillations are decribed by the string equation

$$\rho\ddot{u} = Tu'',$$

where ρ is the string mass per unit length, T is the tension, assumed constant along the string, $u = u(s,t)$ is the transverse displacement, dots denote differentiation with respect to time t, and primes denote differentiation with respect to the arclength s.

The boundary conditions, are, obviously,

$$u_A = u_B = 0.$$

A discretized string equation looks as follows

$$\ddot{u} = v_t^2 \frac{u_{k+1} - 2u_k + u_{k-1}}{\Delta s^2},$$

where $v_t = \sqrt{T/\rho}$ is the transverse wave velocity, u_k is the transverse displacement at the node k, Δs is the distance between the neighboring nodes,

$$\Delta s = \frac{L}{N},$$

N is the number of nodes, and L is the length of the string.

Partial solutions representing the natural modes of oscillations are found in the form

$$u_k = \sin(\Omega_n t)\, \sin(\pi n \xi_k), \qquad n = 1, 2, \ldots$$

where Ω_n are the eigenfrequencies, and $\xi_k = k/N$, $k = 0, 1, \ldots, N$.

Substituting this form of solution into the discretized string equation, we find that the eigenfrequencies of the discretized problem are equal to

$$\Omega_n = 2N \frac{v_t}{L} \sin\left(\frac{\pi n}{2N}\right) \approx \pi n \frac{v_t}{L}\left(1 - \frac{\pi^2 n^2}{24N^2}\right).$$

The exact eigenefrequency obtained from the original partial differential equation is equal to

$$\Omega_n^* = \pi n \frac{v_t}{L}.$$

The relative difference is

$$\frac{\Omega_n - \Omega_n^*}{\Omega_n^*} \approx -\frac{1}{24}\left(\frac{\pi n}{N}\right)^2.$$

Because of the difference in eigenefrequencies, the phase difference between the simulated and exact solutions will accumulate with time as $\Delta\varphi = (\Omega_n - \Omega_n^*)t$. If we need to simulate the excitation of the n-th mode with a relative accuracy ε_n over a period of time Δt, then the difference between the eigenefrequencies must be limited as

$$|\Omega_n - \Omega_n^*| < \frac{\varepsilon_n}{\Delta t}.$$

To satisfy this relation, the number of nodes must be at least

$$N \gtrsim \pi n \sqrt{\frac{\pi n\, v_t \Delta t}{24 L\, \varepsilon_n}}.$$

For a typical momentum exchange system with $L = 90$ km and $v_t = 1$ km/s, it takes at least 125 nodes to maintain an accuracy of 1% for the first mode of transverse oscillations over one 3-hour orbit.

If an explicit integration scheme is used, then the time step will be limited by the condition of stability of the numerical solution. In general, this restriction has a form of

$$\Delta t < k_t \min_i \left\{\frac{\Delta s_i}{v_{ti}}\right\},$$

where k_t is a numeric coefficient depending on the implementation, Δs_i are the distances between the nodes, and v_{ti} are the maximum transverse wave velocities (13) between the corresponding nodes.

By comparison, in a lumped mass model, the time step is limited by

$$\Delta t < k_e \min_i \left\{\frac{\Delta s_i}{v_{ei}}\right\},$$

where k_e is a numeric coefficient depending on the implementation, and v_{ei} are the maximum longitudinal wave velocities (13) between the corresponding nodes.

The longitudinal wave velocity is much higher than the transverse wave velocity, and therefore the time step will be much smaller. This is why simulations based on the Minakov's form of the equations of motion are much faster than those based on lumped mass models.

Two numerical models were implemented, one using Minakov's form of the equations, and the other using a lumped mass model. With a sufficient number of nodes, as explained above, the results of the simulations were consistent between the models within the required accuracy. As expected, the Minakov's type model was by an order of magnitude faster than the lumped mass model.

7. RESONANT EXCITATION

It has been noted in simulations that the transverse oscillations of a typical momentum exchange system go through cycles of a long-term amplitude modulation, when the amplitude first builds up during a number of consecutive perigee passages, and then decreases again.

Fig. 3 shows a history of the transverse amplitude variations over the course of twelve orbits. The amplitude profile is shown in light gray, while the perigee passages are marked with black clusters underneath.

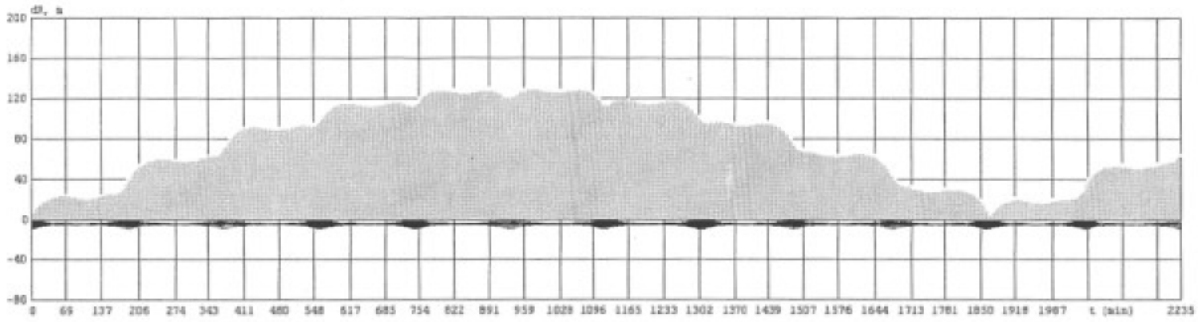

Fig. 3. Resonant excitation of the transverse oscillations.

We see that even without the initial excitation the amplitude of transverse oscillations steadily grows during five perigee passages until it reaches a relatively high level of over 120 m, stays at this level for another perigee passage, and then steadily decreases during the next five perigee passages. This cycle repeats with minor variations.

An in-depth analysis of this phenomenon based on the modal formulation developed in the first part of this report reveals that the mechanism of this excitation is resonant in nature and is caused by a sharp tuning between the natural frequency of the main mode of transverse oscillations U_2 and the frequency of the gravity gradient variation, which cycles twice per every rotation of the tether system about its center of mass.

This tuning is persistent in the sense that the parameters of the tether system must be changed radically to get away from the resonance. In particular, changing the spin rate has very little effect because the transverse frequencies are proportional to the spin rate, as shown in [1].

The modal formulation of Part I accurately describes the motion of the tether system in general and the resonant excitation of transverse oscillations in particular, when the term $\mathbf{Q}_n$ in the main modal equation (37) derived in Part I is used in its general form (38). The simplifications of the term $\mathbf{Q}_n$ demonstrated for a special case of an ideally tapered tether should remain restricted to this special case and should not be applied in case when the MXER tether is not carrying the full load for which it was designed.

For practical purposes, the modal solution requires very few modes and is computed much faster than the numeric solutions based on the Minakov's formulation, not to mention lumped mass models.

8. SENSITIVITY TO NON-GRAVITATIONAL PERTURBATIONS

8.1. Method of Computation.

To evaluate the sensitivity of the motion of the momentum exchange system to non-gravitational perturbations, we use the modal decomposition method described in Part I of this study [1].

As shown in [1], the effect of non-gravitational forces on the excitation of the eigenform U_n is determined by a generalized force

$$\mathbf{\Phi}_n = \mathbf{F}_A U_{nA} + \mathbf{F}_B U_{nB} + \sum_k \mathbf{F}_k U_{nk} + \int_A^B \mathbf{F}\, U_n\, ds. \tag{46}$$

It is computationally expensive to calculate the integral of $\mathbf{F}\, U_n$ over the entire tether length on each step. To make this calculation more efficient, we will use the following quadratic approximation on each tether segment $s_k \le s \le s_{k+1}$

$$\mathbf{F}(s,t) = (2\xi^2 - \xi)\,\mathbf{F}(s_k,t) + (1-4\xi^2)\,\mathbf{F}(s_{k+1/2},t) + (\xi + 2\xi^2)\,\mathbf{F}(s_{k+1},t), \tag{47}$$

where $\xi = (s - s_{k+1/2})/(s_{k+1} - s_k)$, and $s_{k+1/2} = (s_k + s_{k+1})/2$ is the middle of the segment, so that $-1/2 \le \xi \le 1/2$.

Using approximation (47), we have

$$\int_A^B \mathbf{F}\, U_n\, ds = \sum_k \mathbf{Q}_{nk}, \tag{48}$$

where

$$\mathbf{Q}_{nk} = \int_k^{k+1} \mathbf{F}\, U_n\, ds =$$
$$(2I^2_{nk} - I^1_{nk})\,\mathbf{F}(s_k,t) + (I^0_{nk} - 4I^2_{nk})\,\mathbf{F}(s_{k+1/2},t) + (I^1_{nk} + 2I^2_{nk})\,\mathbf{F}(s_{k+1},t),$$

and

$$I^0_{nk} = \int_k^{k+1} U_n ds, \qquad I^1_{nk} = \int_k^{k+1} U_n \xi \, ds, \qquad I^2_{nk} = \int_k^{k+1} U_n \xi^2 ds.$$

The coefficients I^m_{nk} can be precomputed before a simulation run, and to calculate the generalized forces (46), we would need to evaluate the environmental parameters only at the locations of the end masses and embedded masses and at the middle of each tether segment.

With typical parameters, the accuracy of this presentation of the generalized non-gravitational forces meets or exceeds precision requirements for modeling the dynamics of the momentum exchange system.

8.2. Aerodynamic Forces.

As shown in [2], the aerodynamic force acting on a tether segment can be approximated as

$$\mathbf{F} = -\rho_a d_t \gamma \left[|\tau \times \mathbf{v}_a| \left(\left(1 + \frac{\varepsilon}{3}\right) \mathbf{v}_a - \frac{4}{3} \varepsilon \mathbf{v}_\tau \right) + \nu (1 - \varepsilon) |\mathbf{v}_a| (\mathbf{v}_a - \mathbf{v}_\tau) \right], \qquad (49)$$

where d_t is the tether diameter, ρ_a is the air density, $\mathbf{v}_a$ is the tether velocity relative to the air, $\mathbf{v}_\tau = (\mathbf{v}_a, \tau)\tau$ is the component of the velocity $\mathbf{v}_a$ along the tether line, and ε and ν are small parameters, $0 < \varepsilon, \nu \lesssim 0.1$.

The aerodynamic forces acting on the end masses and the embedded masses are calculated as for regular satellites [4].

For a Hoytether [5] consisting of separate strands kept apart from each other, formula (49) must be applied to all individual strands. One must also take into account the overshadowing of the strands. In general, a Hoytether will have a larger total exposed area of the tether and a higher air drag.

With typical system parameters and Hoytethers having between 16 and 24 strands, it has been determined in numerical simulations that a 5% variation in the aerodynamics forces due to air density variations or uncertainties of the aerodynamic parameters of the tether will cause a 2 m shift of the tether tip A after one orbit.

8.3. Ampere Forces.

The Ampere force acting on a tether segment can be represented as

$$\mathbf{F} = I\gamma\tau \times \mathbf{B} \qquad (50)$$

where I is the electric current in the tether, and $\mathbf{B}$ is the geomagnetic induction vector.

Normally, Ampere forces should not be applied during a preparation for a rendezvous. However, to evaluate the sensitivity to the variations of the Ampere forces, we will consider a purely hypothetical situation when there is an electrical "leak" in the system, which results in a very small alternate electric current of a 1 mA amplitude flowing in the conductive segments of the tether in the direction of the EMF and modulated proportionally to the EMF. It was also assumed for simplicity that the "leak" current shuts off at altitudes above 2000 km for the lack of electrons.

It has been observed in simulations that this electric "leak" during the perigee passage causes a 3 m shift of the tether tip A after one orbit.

8.4. Solar Radiation Pressure.

The force of the solar radiation pressure acting on a round tether can be approximated as [2]

$$\mathbf{F} = -p_s d_t \gamma |\boldsymbol{\tau} \times \mathbf{e}_s| \left[\left(1 + \frac{\varkappa}{3}\right) \mathbf{e}_s - \frac{4}{3} \varkappa (\mathbf{e}_s, \boldsymbol{\tau}) \boldsymbol{\tau} \right], \tag{51}$$

where $\mathbf{e}_s$ is a unit vector of the direction to the Sun, p_s is the solar radiation pressure, and $\varkappa$ is the reflection factor.

The solar radiation pressure forces acting on the end masses and the embedded masses are calculated as for regular satellites [4].

For a Hoytether [5] consisting of separate strands kept apart from each other, formula (51) must be applied to all individual strands, taking into account their overshadowing. In general, a Hoytether will have a larger total exposed area of the tether.

With typical system parameters and Hoytethers having between 16 and 24 strands, it has been determined in numerical simulations that a 5% variation in the forces of solar radiation pressure due to uncertainties of the reflective and geometric parameters of the tether will cause a 1 to 4 m shift of the tether tip A after one orbit.

8.5. Thermal Expansion.

Thermal expansion changes the length of the tether segments and thus changes the moment of inertia of the momentum exchange system. The variations of the moment of inertia result in variations of the tether spin rate.

The moment of inertia is proportional to the second power of the average elongation γ_1, and in a simple case of a free rotation, when the angular momentum is conserved, the angular velocity Ω satisfies the relation

$$\gamma_1^2 \Omega = \gamma_0^2 \Omega_0. \tag{52}$$

When the average elongation γ_1 varies with the temperature Θ as

$$\gamma_1 = \gamma_0 + \alpha_t \Delta\Theta, \tag{53}$$

where α_t is the thermal expansion coefficient, then the angular rate will vary as

$$\Delta\Omega \approx -\frac{2\Delta\gamma_1}{\gamma_0}\,\Omega_0 = -\frac{2\alpha_t \Delta\Theta}{\gamma_0}\,\Omega_0.$$

If the average deviation of the actual temperature from the modeled temperature is $\Delta\Theta_{av}$ during a time Δt, then the angle of the tether in-plane orientation will deviate by $\Delta\vartheta = \Delta\Omega_{av}\Delta t$, and the transverse displacement of the tether end A will be estimated as

$$\Delta\vartheta\, L_{AC} \approx -\frac{2\alpha_t \Delta\Theta_{av}}{\gamma_0}\,\Omega_0 \Delta t\, L_{AC},$$

where L_{AC} is the distance from the end A to the center of mass C.

According to [3], Zylon, a candidate tether material, has a negative thermal expansion coefficient of $\alpha_t = -6 \times 10^{-6}$ 1/K. With a typical spin period of 6.3 min and a distance from the end to the mass center of 75 km, we find that after one orbital period of $\Delta t = 3$ hours, the tether end will drift away from its anticipated position by about 163 m per each Kelvin of the average temperature deviation. This sensitivity is attributed to the high spin rate Ω_0.

8.6. Creep.

The average elongation γ_1 will gradually increase with time due to creep,

$$\gamma_1 = \gamma_0 + \alpha_c \Delta t, \tag{54}$$

where α_c is the creep coefficient. In the approximation (52), the average spin rate will be dropping as

$$\Delta\Omega \approx -\frac{2\Delta\gamma_1}{\gamma_0}\,\Omega_0 = -\frac{2\alpha_c \Delta t}{\gamma_0}\,\Omega_0,$$

and the deviation of the angle of the tether in-plane orientation will be growing as

$$\Delta\vartheta \approx -\frac{\alpha_c (\Delta t)^2}{\gamma_0}\,\Omega_0.$$

The transverse displacement of the tether end A will build up with time as

$$\Delta\vartheta\, L_{AC} \approx -\frac{\alpha_c}{\gamma_0}\,\Omega_0 (\Delta t)^2\, L_{AC},$$

where L_{AC} is the distance from the end A to the center of mass C.

As reported in [3], the creep coefficient α_c of Zylon-HM under high stress is on the order of 10^{-6} 1/hour. For a 100-km tether, this will result in tether elongation at a rate of 2.4 m/day. With a typical spin period of 6.3 min and a distance from the end to the mass center of 75 km, we find that after one orbital period of $\Delta t = 3$ hours, the tether end will drift away from its anticipated position by about 41 m. For Zylon-AS, the creep coefficient and the tether end displacement are 3 times higher. As with thermal expansion, this sensitivity is attributed to the high spin rate Ω_0.

8.7. Mass Loss.

There are several processes that will contribute to the variation of the mass of the momentum exchange system:

(1) outgassing
(2) sublimation
(3) micrometeorite damage
(4) hollow cathode emission
(5) molecular deposition (mass addition)

While there is no reliable data on most of them, it has been estimated that a typical momentum exchange system may lose between 5 and 150 grams of its mass per day. As a result of this process, the center of mass of the tether system will be slowly shifting along the tether.

Let us consider the motion of a system with a straight, quasi-rigid tether, whose elements m_i are positioned at points s_i along the line

$$\mathbf{R}_i = \mathbf{R}_C + (s_i - s_C)\,\boldsymbol{\tau}, \tag{55}$$

where $\boldsymbol{\tau}$ is a unit vector, and subscript C refers to the center of mass. By the definition of the center of mass,

$$\sum_i m_i\,(s_i - s_C) = 0. \tag{56}$$

According to (56), when the masses of the elements m_i change, the center of mass slides along the tether at a rate of

$$\dot{s}_C = \frac{1}{M}\sum_i \dot{m}_i\,(s_i - s_C), \tag{57}$$

where M is the total mass of the tether system,

$$M = \sum_i m_i.$$

Differentiating (55) with respect to time, we obtain

$$\ddot{\mathbf{R}}_i = \ddot{\mathbf{R}}_C - \ddot{s}_C \boldsymbol{\tau} - 2\dot{s}_C \dot{\boldsymbol{\tau}} + (s_i - s_C)\ddot{\boldsymbol{\tau}}. \tag{58}$$

Multiplying (58) by m_i and performing summation, we find that

$$\sum_i m_i \ddot{\mathbf{R}}_i = M(\ddot{\mathbf{R}}_C - \ddot{s}_C \boldsymbol{\tau} - 2\dot{s}_C \dot{\boldsymbol{\tau}}), \tag{59}$$

where the terms with $\ddot{\boldsymbol{\tau}}$ canceled out because of the definition of the center of mass (56).

For each element of the system,

$$m_i \ddot{\mathbf{R}}_i = \mathbf{T}_i + \mathbf{F}_i + \mathbf{W}_i, \tag{60}$$

where $\mathbf{T}_i$, $\mathbf{F}_i$, and $\mathbf{W}_i$ are the sums of all internal, external, and reactive forces acting on this element. Substituting equations (60) for the individual elements into (59), we arrive at the following equation of motion of the center of mass

$$\ddot{\mathbf{R}}_C = \ddot{s}_C \boldsymbol{\tau} + 2\dot{s}_C \dot{\boldsymbol{\tau}} + \frac{1}{M} \sum_i (\mathbf{F}_i + \mathbf{W}_i). \tag{61}$$

All internal forces $\mathbf{T}_i$ cancel out after summation, as dictated by the Newton's third law. The terms with the derivatives of s_C describe the perturbation of the orbital motion because of the relocation of the center of mass.

Multiplying (58) by $\boldsymbol{\tau}$ (vector product) and performing summation, we find that

$$J_C \dot{\boldsymbol{\Omega}} = \sum_i (s_i - s_C)\boldsymbol{\tau} \times (\mathbf{F}_i + \mathbf{W}_i), \tag{62}$$

where J_C is the moment of inertia about the center of mass

$$J_C = \sum_i m_i (s_i - s_C)^2,$$

and $\boldsymbol{\Omega}$ is the angular velocity of the tether rotation

$$\boldsymbol{\Omega} = \boldsymbol{\tau} \times \dot{\boldsymbol{\tau}}.$$

It is interesting to note that even though the moment of inertia J_C is changing because of the mass loss, it does not directly result in the variation of the angular velocity, unlike the case of creep and thermal expansion.

While the hollow cathodes are expected to create a small torque of reactive forces $\mathbf{W}_i$, it is not obvious that the other processes involved in the mass exchange

with the environment will be anisotropic enough to create any noticeable torque of the reactive forces.

Assuming that the reactive torques are negligible, the gravitational field is Newtonian, and the non-gravitational forces are small, the in-plane perturbation of the orbit of the center of mass can be described, according to (61), as

$$\begin{aligned} \delta\ddot{x} - 2\omega\,\delta\dot{y} - \dot{\omega}\,\delta y - \left(\omega^2 + \frac{2\mu_E}{R_C^3}\right)\delta x &= \ddot{s}_C\cos\vartheta - 2\dot{s}_C\,\Omega\sin\vartheta, \\ \delta\ddot{y} + 2\omega\,\delta\dot{x} + \dot{\omega}\,\delta x - \left(\omega^2 - \frac{\mu_E}{R_C^3}\right)\delta y &= \ddot{s}_C\sin\vartheta + 2\dot{s}_C\,\Omega\cos\vartheta, \end{aligned} \tag{63}$$

where δx and δy are the vertical and horizontal displacements of the, center of mass, ω is the orbital angular rate, Ω is the spin rate, and ϑ is the angle between the tether and the local vertical. For a fast spinning tether, $\Omega \gg \omega$, we have $\vartheta \approx \Omega t$, and the order of magnitude of the perturbation is estimated as

$$\delta x^2 + \delta y^2 \sim \left(\frac{\ddot{s}_C}{\Omega^2}\right)^2 + \left(\frac{2\dot{s}_C}{\Omega}\right)^2.$$

These displacements are expected to be very small (less than a millimeter) because of the fast spin and slow shift of the center of mass.

9. ESTIMATION AND CONTROL REQUIREMENTS

As shown in the previous section, the position of the tether tip in the momentum exchange system is very sensitive to variations of the system and environmental parameters, when considered from the standpoint of the rendezvous precision requirements.

The variations producing the most impact on the tether tip positioning are related to the lengths of the tether segments, as we have seen in the case of thermal expansion and creep.

If the distances between the neighboring tethered modules could be measured with an accuracy of a few millimeters, then we could use this information to significantly improve the estimate of the current state of the momentum exchange system.

Every dynamic process in the momentum exchange system, one way or another, leaves its signature in the longitudinal motion of the tether. Using a detailed dynamic model, we may be able translate a continuous stream of precise distance measurements, combined with other data, into a reasonably accurate estimation of the tether system state.

Furthermore, using the information about the system state, we could compensate for some unexpected (or unmodeled) deviations from the projected path. In particular, deviations of the rotation about the center of mass could be corrected by slightly varying the tether length(s) or changing the mass distribution of the end bodies or power stations.

Given extremely short rendezvous windows with very fast relative motions, and various inherent uncertainties of the environment, it is very clear that elaborate estimation and control algorithms must be developed to make successful rendezvous with the momentum exchange system possible.

10. CONCLUSIONS

The task of prediction of the motion of a momentum exchange system with a 9-digit accuracy is extremely challenging, and it is relentlessly testing our ability to gain fundamental insights into the nature of the tether dynamics in this system.

It has been shown that the modal decomposition approach developed in the first part of this study is a very powerful and precise tool for the simulation of the dynamics of momentum exchange tethers.

However, to get a prediction with the required accuracy using this tool, one must have precise inputs, including the initial state, system parameters, and the environmental models. In simulations, the tether tip positioning has been observed to be quite sensitive to even small variations of the parameters involved in the calculations.

It is therefore imperative that precise estimation and control algorithms be developed to compensate for the inevitable uncertainties and support high precision rendezvous.

REFERENCES

1. LEVIN, E.M., MXER Simulation Study, Part I, MSFC Contract Report, January 10, 2005.
2. BELETSKY, V.V. AND LEVIN, E.M. Dynamics of Space Tether Systems. *Advances in the Astronautical Sciences,* AAS, **83,** 1993, Univelt, Inc.
3. PBO FIBER ZYLON, Technical Information, Toyobo Co., Ltd., Japan, 2001.
4. MONTENBRUCK, O. AND GILL, E. *Satellite Orbits: Models, Methods and Applications,* Springer Verlag, 2000.
5. HOYT, R.P., SLOSTAD, J.T. AND FRANK, S.S. A Modular Momentum-Exchange Electrodynamic-Reboost Tether System Architecture, AIAA-2003-5214, 2003.

REPORT DOCUMENTATION PAGE

Form Approved
OMB No. 0704-0188

1. AGENCY USE ONLY *(Leave Blank)*	2. REPORT DATE	3. REPORT TYPE AND DATES COVERED
	June 2006	Contractor Report

4. TITLE AND SUBTITLE
Dynamics Simulation Model for Space Tethers

5. FUNDING NUMBERS
NNM04AB51C

6. AUTHORS
E.M. Levin, J. Pearson, and J.C. Oldson

7. PERFORMING ORGANIZATION NAME(S) AND ADDRESS(ES)
Star Technology and Research, Inc.
3213 Carmel Bay Drive, Suite 200
Mout Pleasant, SC 29466-8513

8. PERFORMING ORGANIZATION REPORT NUMBER
M–1164

9. SPONSORING/MONITORING AGENCY NAME(S) AND ADDRESS(ES)
Dr. Joseph A. Bonometti, Emerging Technologies Manager
In-Space Propulsion
George C. Marshall Space Flight Center
Marshall Space Flight Center, Alabama 35812

10. SPONSORING/MONITORING AGENCY REPORT NUMBER
NASA/CR—2006–214432

11. SUPPLEMENTARY NOTES
Prepared for Emerging Propulsion Technologies
In-Space Propulsion Technology Project

12a. DISTRIBUTION/AVAILABILITY STATEMENT
Unclassified-Unlimited
Subject Category 13
Availability: NASA CASI 301–621–0390

12b. DISTRIBUTION CODE

13. ABSTRACT *(Maximum 200 words)*

This document describes the development of an accurate model for the dynamics of the Momentum Exchange Electrodynamic Reboost (MXER) system. The MXER is a rotating tether about 100-km long in elliptical Earth orbit designed to catch payloads in low Earth orbit and throw them to geosynchronous orbit or to Earth escape. To ensure successful rendezvous between the MXER tip catcher and a payload, a high-fidelity model of the system dynamics is required. The model developed here quantifies the major environmental perturbations, and can predict the MXER tip position to within meters over one orbit.

14. SUBJECT TERMS
space tethers, dynamics, estimation, control, orbit propagation, perturbations, drag, outgassing, thermal effects

15. NUMBER OF PAGES
66

16. PRICE CODE

17. SECURITY CLASSIFICATION OF REPORT	18. SECURITY CLASSIFICATION OF THIS PAGE	19. SECURITY CLASSIFICATION OF ABSTRACT	20. LIMITATION OF ABSTRACT
Unclassified	Unclassified	Unclassified	Unlimited

National Aeronautics and
Space Administration
IS20
George C. Marshall Space Flight Center
Marshall Space Flight Center, Alabama
35812